Article

Allele-selective lowering of mutant HTT protein by HTT–LC3 linker compounds

https://doi.org/10.1038/s41586-019-1722-1

Received: 5 February 2019

Accepted: 24 September 2019

Published online: 30 October 2019

Zhaoyang Li[1,9], Cen Wang[1,9], Ziying Wang[1,9], Chenggang Zhu[2,9], Jie Li[3], Tian Sha[1], Lixiang Ma[4], Chao Gao[5], Yi Yang[6], Yimin Sun[1], Jian Wang[1], Xiaoli Sun[1], Chenqi Lu[1], Marian Difiglia[7], Yanai Mei[1], Chen Ding[1,10], Shouqing Luo[6,10], Yongjun Dang[8], Yu Ding[1]*, Yiyan Fei[2]* & Boxun Lu[1]*

Accumulation of mutant proteins is a major cause of many diseases (collectively called proteopathies), and lowering the level of these proteins can be useful for treatment of these diseases. We hypothesized that compounds that interact with both the autophagosome protein microtubule-associated protein 1A/1B light chain 3 (LC3)[1] and the disease-causing protein may target the latter for autophagic clearance. Mutant huntingtin protein (mHTT) contains an expanded polyglutamine (polyQ) tract and causes Huntington's disease, an incurable neurodegenerative disorder[2]. Here, using small-molecule-microarray-based screening, we identified four compounds that interact with both LC3 and mHTT, but not with the wild-type HTT protein. Some of these compounds targeted mHTT to autophagosomes, reduced mHTT levels in an allele-selective manner, and rescued disease-relevant phenotypes in cells and in vivo in fly and mouse models of Huntington's disease. We further show that these compounds interact with the expanded polyQ stretch and could lower the level of mutant ataxin-3 (ATXN3), another disease-causing protein with an expanded polyQ tract[3]. This study presents candidate compounds for lowering mHTT and potentially other disease-causing proteins with polyQ expansions, demonstrating the concept of lowering levels of disease-causing proteins using autophagosome-tethering compounds.

Lowering the levels of disease-causing proteins, especially those with unknown activities, is an emerging approach for disease treatment. Biological tools such as RNA-mediated inhibition (RNAi) or CRISPR may achieve this goal[4–6], but their clinical delivery is challenging. Enhancing proteasomal degradation of target proteins using proteolysis-targeting chimeric molecules (PROTACs) is a promising emerging approach[7], but proteasomes alone are inefficient in degrading certain large proteins or aggregates[8]. Macroautophagy (hereafter referred to as autophagy), an independent protein-degradation pathway, is a bulk degradation system that engulfs proteins into autophagosomes for subsequent lysosomal degradation[9]. Autophagy is present in all eukaryotic cells, and therefore harnessing the power of autophagy to degrade certain target proteins may have potential for drug discovery. Here we investigate this possibility in the context of lowering mHTT, which contains a polyQ stretch with at least 36 glutamine residues and causes Huntington's disease, an incurable monogenetic neurodegenerative disorder[2].

mHTT could be degraded by autophagy, during which protein substrates are incorporated into double-membrane autophagosomes associated with lipidated LC3[1]. We therefore hypothesized that linker compounds that interact with both mHTT and LC3 may tether the molecules together to enhance recruitment of mHTT into autophagosomes, facilitating its degradation. In addition, mHTT–LC3 linker compounds that do not interact with wild-type HTT (wtHTT) may promote allele-selective degradation of mHTT. Because no mHTT–LC3-interacting compounds have been reported, we performed small-molecule-microarray (SMM)-based screening for such compounds and used wtHTT for the counter-screen to identify allele-selective candidates.

Results

Identification of mHTT–LC3 linker compounds

We stamped 3,375 compounds (Fig. 1a) in duplicate onto a microarray on isocyanate-functionalized glass slides using the nucleophile-isocyanate reaction, which forms covalent bonds between the compounds and the glass slides[10,11]. We then purified the human LC3B protein[1] (Extended Data Fig. 1a, b, Supplementary Table 1), a pathogenic mHTT exon1 fragment[12] with an expanded polyQ region containing 72 glutamines (mHTTexon1(Q72)), and a control wtHTT exon1 fragment

[1]Neurology Department at Huashan Hospital, State Key Laboratory of Medical Neurobiology and MOE Frontiers Center for Brain Science, Institutes of Brain Science, School of Life Sciences, Fudan University, Shanghai, China. [2]Department of Optical Science and Engineering, Shanghai Engineering Research Center of Ultra-Precision Optical Manufacturing, Key Laboratory of Micro and Nano Photonic Structures (Ministry of Education), Fudan University, Shanghai, China. [3]Large-scale Preparation System, National Facility for Protein Science in Shanghai, Shanghai, China. [4]Department of Anatomy, Histology and Embryology, Shanghai Medical College, Fudan University, Shanghai, China. [5]Institutes of Biomedical Sciences, Fudan University, Shanghai, China. [6]Peninsula Schools of Medicine and Dentistry, Institute of Translational and Stratified Medicine, University of Plymouth, Plymouth, UK. [7]Laboratory of Cellular Neurobiology, Department of Neurology, Massachusetts General Hospital, Charlestown, MA, USA. [8]Key Laboratory of Metabolism and Molecular Medicine, Ministry of Education, Department of Biochemistry and Molecular Biology, School of Basic Medical Sciences, Fudan University, Shanghai, China. [9]These authors contributed equally: Zhaoyang Li, Cen Wang, Ziying Wang, Chenggang Zhu. [10]These authors jointly supervised this work: Chen Ding, Shouqing Luo. *e-mail: yuding@fudan.edu.cn; fyy@fudan.edu.cn; luboxun@fudan.edu.cn

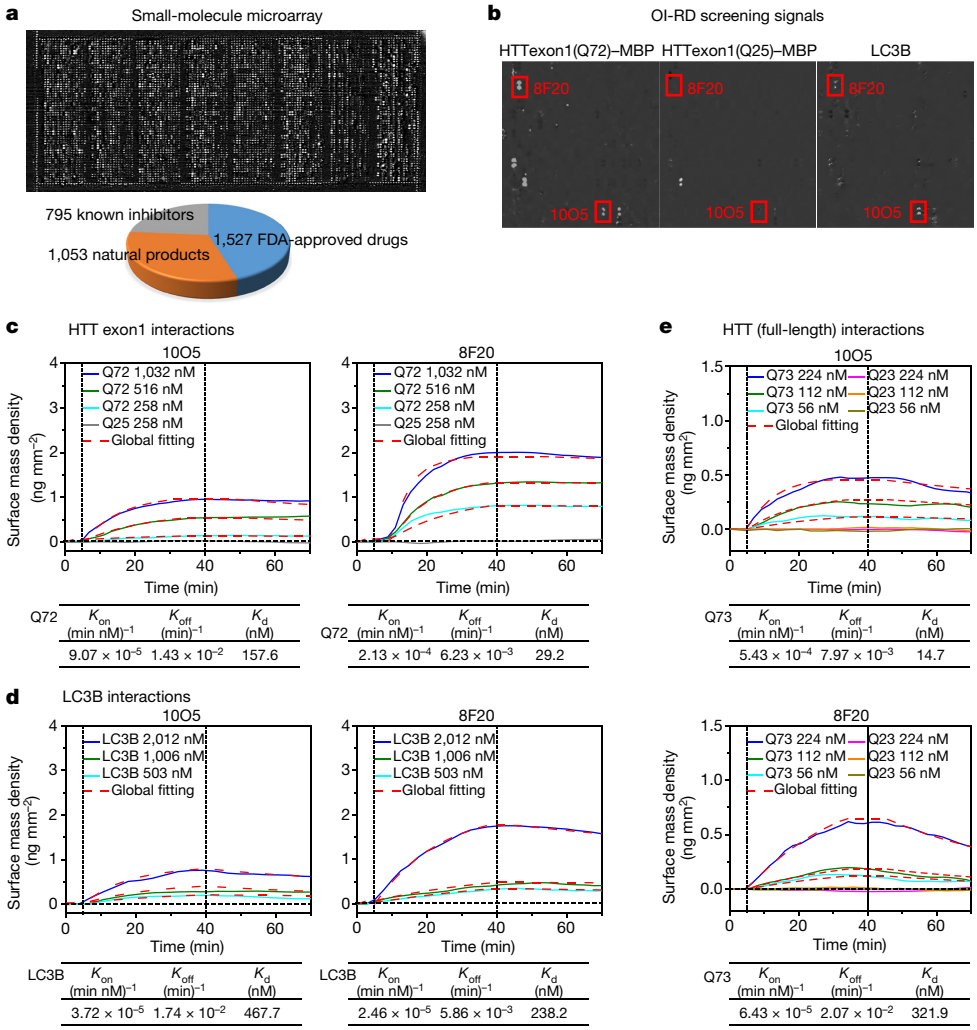

Fig. 1 | Identification of potential mHTT–LC3 linker compounds by SMM-based screening and validation. a, OI-RD image of a SMM. Each compound was printed in duplicate in adjacent vertical positions. **b**, Magnified view of surface mass-density changes after incubation with HTTexon1(Q25)–MBP, HTTexon1(Q72)–MBP or LC3B. The red outlines highlight two hits (10O5 and 8F20). **c**–**e**, Association–dissociation curves of surface-immobilized compounds 8F20 and 10O5 with HTTexon1(Q72)–MBP (Q72) (**c**), LC3B (**d**) and full-length HTT(Q73) (Q73) (**e**) at the indicated purified protein concentrations. In association–dissociation curves, vertical dashed lines mark the starts of association and dissociation phases of the binding event. The red dashed curves are global fits to a Langmuir reaction model with the fitting parameters listed at the bottom of each plot. No binding signals were observed for HTTexon1(Q25)–MBP or full-length HTT(Q23) proteins, and thus these parameters are not presented.

(HTTexon1(Q25)) (Extended Data Fig. 1c, d) for the screen. We fused a maltose-binding protein (MBP) tag to both HTT exon1 proteins to increase their solubility for subsequent experiments.

To identify compounds that interact with LC3B and mHTT, we incubated these proteins over the SMMs and detected compound–protein interactions using a scanning oblique-incidence reflectivity difference (OI-RD) microscope[13–18], an optical biosensor. We then performed experiments with HTTexon1(Q25) or buffer alone to exclude nonspecific signals, and identified two compounds, 10O5 (GW5074, 3-3-((3,5-dibromo-4-hydroxyphenyl)methylidene)-5-iodo-1*H*-indol-2-one) and 8F20 (ispinesib, *N*-(3-aminopropyl)-*N*-((1*R*)-1-(7-chloro-4-oxo-3-(phenylmethyl)-2-quinazolinyl)-2-methylpropyl)-4-methylbenzamide), that interact with both LC3B and mHTTexon1(Q72), but not with HTTexon1(Q25) (Fig. 1b, annotation based on the ID in the compound library). We then measured the on and off rates (K_{on} and K_{off}, respectively) of these interactions to confirm our observation (Fig. 1c, d), finding that both compounds showed dissociation constants (K_d) of around 100 nM with LC3B or mHTTexon1(Q72). As shown in Fig. 1e, these compounds also interacted with the full-length mHTT (flHTT(Q73), Extended Data Fig. 1e), but not with wild-type HTT (HTTexon1(Q25) or flHTT(Q23), Fig. 1c, e) or irrelevant proteins (Extended Data Fig. 2a) including MBP–His_8 (MBP), superfolder GFP (sfGFP) and Rpn10 (a proteasomal ubiquitin receptor) (Extended Data Fig. 1f). We then validated the interaction using an orthogonal assay, microscale thermophoresis (MST), and obtained consistent results (Extended Data Fig. 2b).

Linkers induced allele-selective mHTT lowering

We then tested whether these potential mHTT–LC3 linker compounds decrease mHTT levels via autophagy as predicted. Both compounds decreased levels of mHTT in cultured primary cortical neurons from a well-established HD-knock-in mouse model ($Hdh^{Q7/Q140}$)[19] (Fig. 2a), but had little or no effect on levels of wtHTT in the heterozygous HD neurons ($Hdh^{Q7/Q140}$) (Fig. 2a) or wild-type neurons ($Hdh^{Q7/Q7}$) (Fig. 2b), consistent with the lack of interaction of these compounds with wtHTT. We then screened for other mHTT–LC3 linker compounds on the basis of common features of the two hit compounds 10O5 and 8F20. The hydroxyl group in 10O5 and the amino group in 8F20 were used in the nucleophile-isocyanate reaction for stamping of the SMMs, and these groups were inaccessible to mHTT and LC3B for the compound–protein

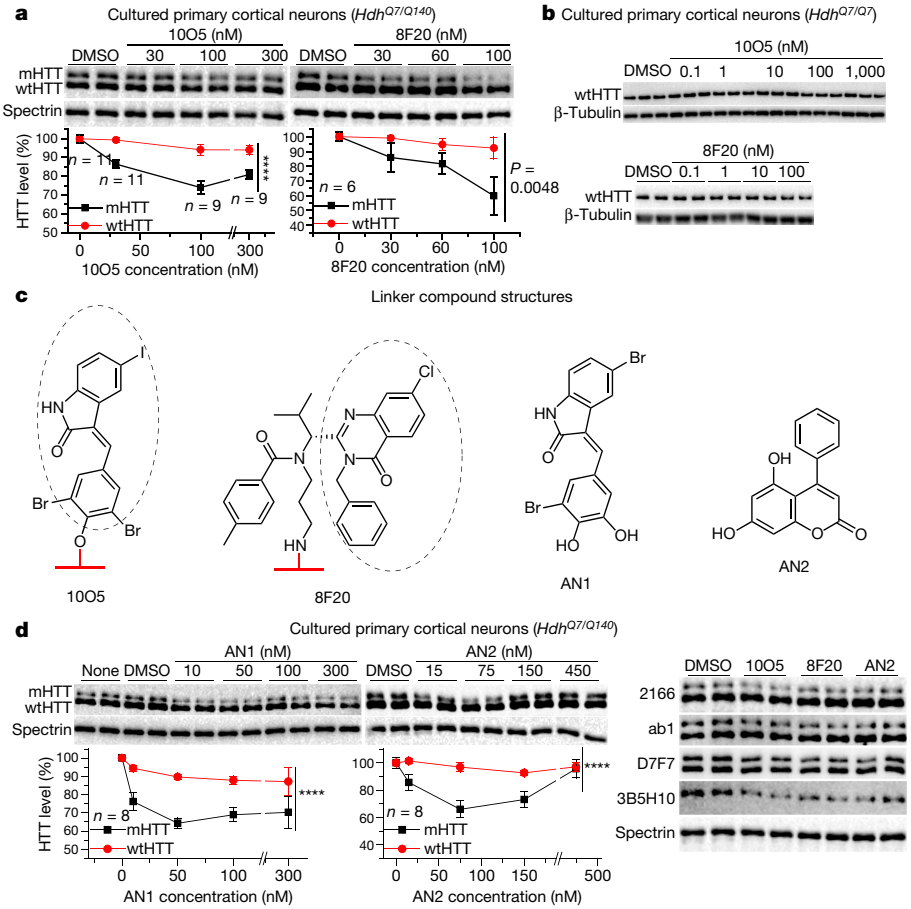

Fig. 2 | mHTT–LC3 linker compounds lower mHTT but not wtHTT in cultured mouse neurons via autophagy. a, Western blot (HTT detected by the 2166 antibody) and quantification of compound-treated cultured cortical neurons from $Hdh^{Q7/Q140}$ HD-knock-in mice. Two-way ANOVA. For 10O5, $F(1, 72) = 50.93$, $P < 0.0001$; for 8F20, $F(1, 40) = 8.903$, $P = 0.0048$. **b**, Representative western blots (from three biological repeats) of cultured wild-type cortical neurons treated with the indicated compounds. **c**, Two-dimensional structures of the hit compounds and the other identified effective linker compounds. The red lines indicate the glass chip surface on which the compounds are immobilized. The dotted ovals indicate the possible chemical groups exposed for protein–compound interactions in the screening. **d**, Left and middle, as in **a**, but using AN1 or AN2. For AN1, $F(1, 70) = 32.96$, $P < 0.0001$; for AN2, $F(1, 69) = 23.03$, $P < 0.0001$. Right, as in **a**, but blotted with indicated HTT antibodies (10O5 and 8F20: 100 nM; AN2: 50 nM). For all panels, *n* indicates the number of independently plated wells; data are mean ± s.e.m. Full blots of cropped gels are shown in Extended Data Fig. 3b or Supplementary Fig. 1.

interaction during the screening (Fig. 2c). Thus, whereas the two hit compounds have different structures, the exposed chemical groups on the SMMs share similarities in that they contain an aryl ring connected to a lactam-based bicyclic structure with halogen-substituted aryl group (Fig. 2c). We tested several compounds with similar features and identified two additional mHTT–LC3 linker compounds (Fig. 2c, AN1 (3-5-bromo-3-((3-bromo-4,5-dihydroxyphenyl)methylidene)-1*H*-indol-2-one) and AN2 (5,7-dihydroxy-4-phenylcoumarin), which interact with both mHTT and LC3B but not with wtHTT or irrelevant control proteins (Extended Data Fig. 2c, d). They also reduced the levels of mHTT in an allele-selective manner in cultured HD mouse neurons (Fig. 2d). No cytotoxicity was observed in cultured neurons treated with these compounds at the tested concentration range (Extended Data Fig. 2e), confirming that the reduction in mHTT was not due to cell loss.

Most of these compounds showed an optimal dose (hook effect) in lowering mHTT (Fig. 2a, d): a sufficient concentration is desired for tethering mHTT and LC3 together, but excessively high concentrations may cause the compound molecules to interact with mHTT and LC3 separately without tethering them. Similar concentration-dependent effects were observed in fibroblasts of patients with HD (Fig. 3c, right) and have been reported for PROTAC[20]. Consistent with the prediction that the reduction in mHTT is mediated by degradation via autophagy, the autophagy inhibitor NH_4Cl or chloroquine blocked the mHTT-lowering effects (Extended Data Fig. 3a), confirming that the compounds targeted mHTT for autophagic degradation. Further, the compound-induced mHTT-lowering effects were only slightly enhanced by the mTOR inhibitor rapamycin, an enhancer of autophagosome formation (Extended Data Fig. 3a, right; also see Fig. 3b).

The reduction of mHTT levels could be detected by multiple mHTT antibodies—including 3B5H10, which detects a toxic species of the expanded polyQ stretch[21,22] (Fig. 2d, right)—suggesting that the detected reduction of the mHTT signal was not due to changes in affinity to a specific antibody. In addition, we did not observe any obvious increase of possible polyQ-containing mHTT fragments at lower molecular weights (Extended Data Fig. 3b, c), suggesting that the reduced levels of mHTT were not a result of increased site-specific cleavages of mHTT.

We further investigated the effects of the compounds in cells from patients with HD using the well-established homologous time-resolved fluorescence (HTRF) assay[23,24], which is more quantitative than western blots but is not applicable to mouse mHTT proteins owing to non-specific signals[25]. We observed autophagy-dependent lowering of mHTT by these compounds in fibroblasts from patients with HD and neurons derived from induced pluripotent stem cells (iPS cells) (Fig. 3a, b, Extended Data Fig. 3d), but no lowering of wtHTT in fibroblasts from healthy human donors or patients with Parkinson's disease

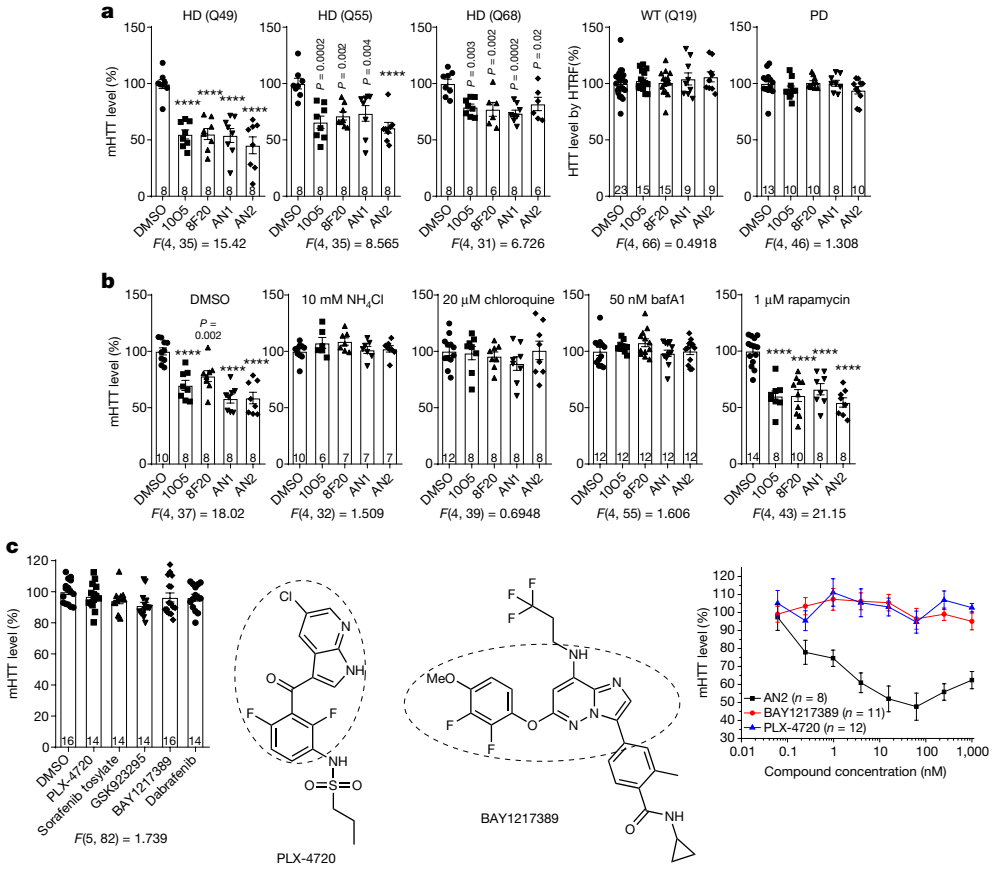

Fig. 3 | mHTT–LC3 linker compounds lower mHTT in cells from patients with HD. a, HTT levels measured by HTRF (2B7/MW1 for mHTT, and 2B7/2166 for total HTT) in primary fibroblasts from patients with HD, wild-type controls (WT) or patients with Parkinson's disease (PD) who were treated with the indicated compounds (100 nM). All signals were normalized to the average signals from the DMSO control group. One-way ANOVA with post hoc Dunnett's tests. ****$P < 0.0001$. **b**, As in **a**, but using immortalized fibroblasts treated with or without the autophagy inhibitors NH_4Cl, chloroquine or bafA1, or the autophagy enhancer rapamycin. **c**, Left, as in **a**, but using immortalized fibroblasts from patients with HD (expressing mHTT(Q47)), treated with indicated c-Raf or KSP inhibitors at 100 nM. Middle, 2D structure of the inhibitors. The dotted ovals indicate the parts of the compounds that share similarities with the hit compounds. Right, dose-response curves of the indicated compounds. For all panels, *n* indicates the number of independently plated wells; data are mean ± s.e.m.

(Fig. 3a). To further confirm the role of autophagic degradation, we tested the effects of the compounds with or without lowering of *ATG5*, a key autophagy gene that is required for autophagosome formation[26]. ATG5 knockdown in fibroblasts from a patient with HD (expressing mHTT(Q47)) significantly decreased LC3-II levels and nullified the mHTT-lowering effects induced by the mHTT–LC3 linker compounds (Extended Data Fig. 3e). Similar results were obtained in ATG5-knockout mouse embryonic fibroblasts[26] (MEFs, Extended Data Fig. 3f), confirming that the effects of the compounds were mediated by autophagic degradation.

The two hit compounds 10O5 and 8F20 are known to inhibit c-Raf and KSP[27,28], respectively, whereas AN1 and AN2 had unknown activities on these targets. We therefore tested their potential influence on c-Raf and KSP. On the basis of the in vitro c-Raf kinase assay, 10O5 (a known c-Raf inhibitor)—but not the other three compounds—inhibited c-Raf at the concentrations tested (Extended Data Fig. 4a). We then tested MEK and ERK phosphorylation levels in the cultured neurons treated with these compounds at optimal mHTT-lowering concentrations to evaluate Raf activity[29] and found no significant effects of all tested compounds (Extended Data Fig. 4b, left). We also tested phospho-BUBR1 levels to evaluate KSP activity[30], and again observed no significant effects (Extended Data Fig. 4b, right). We made similar observations in fibroblasts (expressing mHTT(Q47)) from a patient with HD (Extended Data Fig. 4c). Thus, the observed reduction in mHTT is probably irrelevant to c-Raf or KSP inhibition. To further confirm this, we examined the effects of several known c-Raf or KSP inhibitors, and found that they had no HTT-lowering effects (Fig. 3c, left). Two of these inhibitors, PLX-4720 and BAY1217389, have structures similar to 10O5 and 8F20, respectively (Fig. 3c, middle). These compounds did not lower mHTT in cells from patients at sub-micromolar concentrations (Fig. 3c, right), probably because they had very weak affinity to LC3 and mHTT, if any (Extended Data Fig. 2c, right). By contrast, AN2 reduced mHTT levels in the same cells in a dose-dependent manner (Fig. 3c, right).

We then investigated the effects of the compounds in vivo. Because the *Drosophila* LC3 homologue Atg8 has a predicted structure that is highly similar to LC3B (Extended Data Fig. 5a), we tested the compounds in a HD transgenic fly model expressing human full-length mHTT. All of the mHTT–LC3 linker compounds that we identified significantly reduced mHTT levels in *Drosophila* (Extended Data Fig. 5b), validating the in vivo efficacy of these compounds.

We further investigated the in vivo effects of the compounds using the HD-knock-in mouse model ($Hdh^{Q7/Q140}$)[19] by intracerebroventricular injections. Treatment with three of the four linker compounds (10O5, AN1 or AN2, but not 8F20) led to significant lowering of mHTT in cortices of HD mice (Extended Data Fig. 6a). We then performed intraperitoneal injection of 10O5 and AN2 at 0.5 mg kg^{-1} in HD-knock-in mice. The compounds crossed the blood–brain barrier and reached the brain at detectable concentrations (Extended Data Fig. 5c, approximately

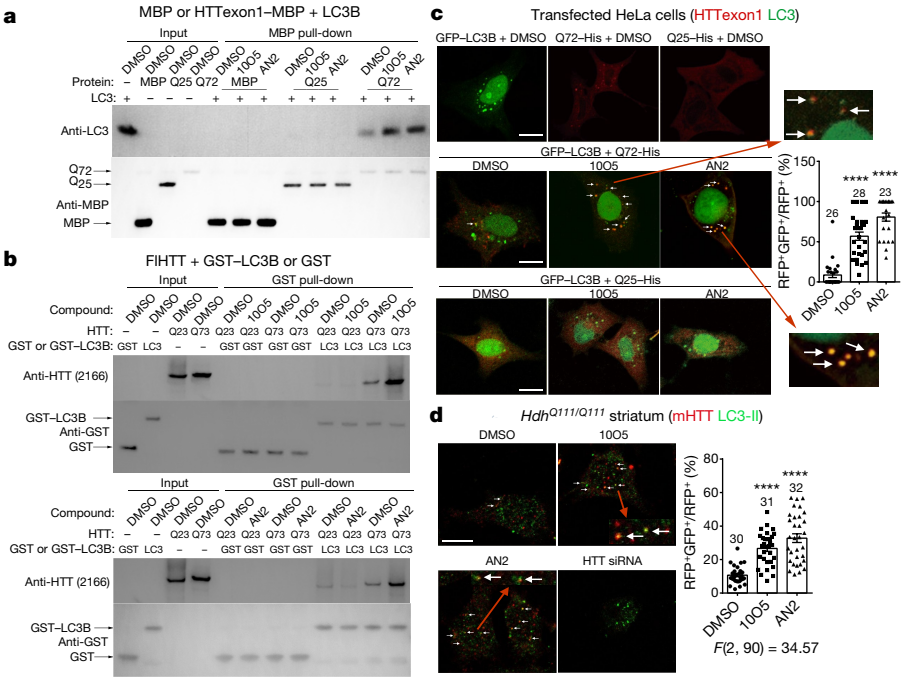

Fig. 4 | Linker compounds enhance the mHTT–LC3 interaction and tether mHTT to autophagosomes. a, **b**, Representative results (from three biological repeats) of in vitro pull-down experiments using purified HTT and LC3B proteins (see Methods for details). **c**, **d**, Representative images (scale bar, 10 μm) and quantification of the co-localization between HTT and autophagosomes in HeLa cells transfected with the indicated cDNA plasmids (**c**) or striatum from *Hdh*$^{Q111/Q111}$ mice (**d**). Data are mean ± s.e.m. *n* indicates the number of cells. One-way ANOVA with post hoc Dunnett's test. ****$P < 0.0001$.

20–200 nM for 10O5 and 20–40 nM for AN2; no signal was detected in the DMSO-injected control group) 0.5–6 h after injection. Consistent with these results, we observed significant allele-selective lowering of mHTT in mouse cortices and striata (Extended Data Fig. 6b, c). The observed lowering was not due to changes in mHTT solubility, because no increase of mHTT aggregates was observed in the cortical tissues of mice treated with these compounds (Extended Data Fig. 6d).

Linkers tether mHTT to autophagosomes

We then examined whether these compounds actually function as linkers between mHTT and LC3 to target mHTT for autophagosome engulfment. The presence of 10O5 or AN2, the two compounds that were effective by intraperitoneal injection in vivo, markedly enhanced the mHTT–LC3 interaction in in vitro pull-down experiments (Fig. 4a, comparing lane 11 with 12 and 13; Fig. 4b, comparing lane 11 with 12, top and bottom). There was no enhancement effect for the wild-type HTT–LC3 interaction (Fig. 4a, lanes 8–10; Fig. 4b, lane 9 and 10, top and bottom). Consistent with this, these compounds led to increased engulfment of mHTT by autophagosomes, both in transiently transfected HeLa cells expressing exogenous GFP–LC3B and in HTTexon1–MBP–His fragments (Fig. 4c), and in mouse striatal cells (ST*Hdh*$^{Q111/Q111}$)[31] expressing endogenous LC3 and full-length mHTT proteins (Fig. 4d).

These data confirmed that the compounds tether mHTT, LC3B and autophagosomes in vitro and in cells, although the detailed structural information remains to be resolved.

Linkers do not influence autophagy function

The lowering of mHTT levels by the linker compounds was unlikely to be a result of enhanced autophagy, because the number and size of autophagosomes remained unchanged (Extended Data Fig. 7a). We further investigated whether the compounds could influence autophagy using established approaches[32–34]. Neither 10O5 nor AN2 influenced the autophagosome–lysosome fusion or autophagy activity (Extended Data Fig. 7b–d). Furthermore, we observed no changes in LC3-II levels in the cultured cortical neurons treated with 10O5 or AN2 in the absence or presence of the lysosome inhibitor bafilomycin A1 (bafA1) (Extended Data Fig. 7e). The level of the known autophagy-selective substrate protein SQSTM1 (also known as p62) was also unaffected in vivo and in cultured neurons (Extended Data Figs. 7f, 8a). In addition, other wild-type polyQ proteins (ATXN3 and TBP) and control proteins (NBR1, NCOA4, actin, GAPDH and tubulin) were not influenced (that is, any change amounted to less than 10%) (Extended Data Fig. 8a).

We then performed proteomics analysis to obtain a more complete overview of proteins that may have been influenced by these compounds. We observed significant lowering (about 20%, $P < 0.01$) of HTT levels in cortices of mice injected intraperitoneally with 10O5 or AN2 (Extended Data Fig. 8b, bar plots). As the proteomics analysis was unable to distinguish mHTT from wtHTT, the actual reduction in mHTT is likely to be higher than this. Meanwhile, using the criteria of $P < 0.01$, we observed changes in only a small percentage of proteins (Extended Data Fig. 8b; see Supplementary Table 2 for details). No autophagy-specific substrate proteins exhibited significant changes and there was no enrichment of proteins associated with the autophagy pathway (Supplementary Table 2), further confirming that autophagy was unaffected. Proteomics analysis in cultured neurons gave consistent results (Extended Data Fig. 8c; see Supplementary Table 3 for details).

Linker compounds depleted expanded polyQ proteins

The linker compounds interacted with and lowered mHTT but not wtHTT (Fig. 1). The simplest explanation for this specificity is that the compounds specifically interact with the expanded polyQ tract, possibly by recognizing its emergent conformation, which is different from that of the short polyQ stretch[21,35]. If so, the linker compounds may also affect other proteins with expanded polyQ regions. Consistent with this prediction, compounds 10O5, AN1 and AN2 reduced the levels of mutant but not wild-type ATXN3 in fibroblasts from patients with spinocerebellar ataxia type 3 (SCA3) (Extended Data Fig. 9a) and

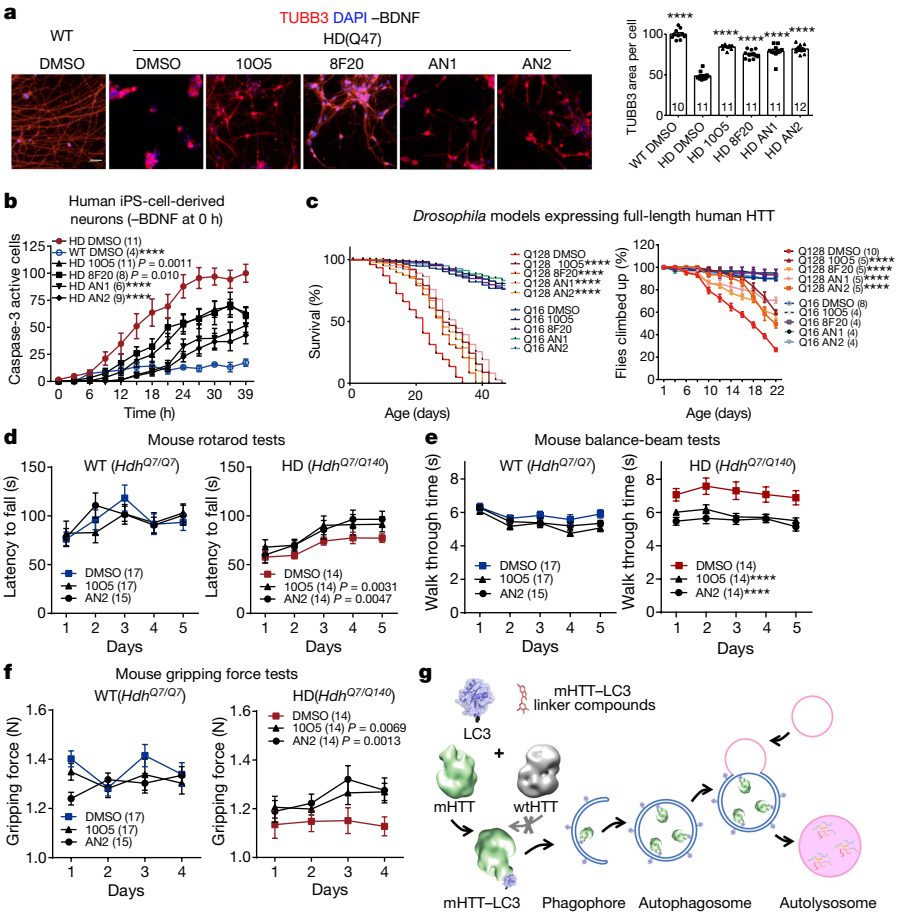

Fig. 5 | Linker compounds rescue HD-relevant phenotypes in cells and in vivo. a, Left, representative DAPI staining and immunostaining of the neuronal-specific tubulin marker TUBB3, showing neuronal morphology of patient iPS-cell-derived striatal neurons (HD: Q47; WT: Q19) treated with indicated compounds. Right, quantification of TUBB3 area per cell. Scale bar, 50 µm. **b**, Neuronal apoptosis at different time points after BDNF removal, measured using a green fluorescent dye (NucView 488) to detect active caspase-3. **c**, Left, Kaplan–Meier survival curves of transgenic *Drosophila* with the indicated transgenes and treatments. Right, climbing performance of the treated transgenic flies as a function of age after eclosion. **d**–**f**, Mouse behavioural tests showing improvement of HD-relevant phenotypes after intraperitoneal injection of the indicated compounds at 0.5 mg kg^{-1}. **g**, A model showing how mHTT–LC3 linker compounds may induce mHTT degradation, illustrating the concept of lowering target protein levels using autophagosome-tethering compounds. The images representing HTT are reproduced from ref. [37] under a CC BY license.

exogenously expressed 72Q–GFP, 46Q–GFP and 38Q–GFP but not 25Q–GFP proteins (containing on Met-polyQ-sfGFP sequences) in HEK293T cells (Extended Data Fig. 9b). These data suggest that the compounds distinguished the expanded polyQ stretch from the short polyQ stretch at a threshold between 25Q and 38Q. To further confirm this, we tested the interactions of these compounds with polyQ motifs (Extended Data Fig. 9c) and confirmed that 10O5, AN1 and AN2 interact with polyQ–GFP with 38 or more glutamine residues, but not 25Q–GFP or GFP alone (Extended Data Figs. 2, 9d, e).

Linker compounds rescued HD-relevant phenotypes

We further investigated the therapeutic potential of the compounds for treating HD. All the mHTT–LC3 linker compounds rescued mHTT toxicity in neurons derived from iPS cells of patients with HD (Fig. 5a, b). They also rescued HD-relevant behavioural deficits and increased the lifespan of flies expressing human mHTT, while having no influence on the flies expressing wtHTT (Fig. 5c).

Finally, we investigated the disease-relevant behavioural phenotypes in ten-month-old heterozygous HD-knock-in mouse (*Hdh*$^{Q7/Q140}$). HD mice exhibited significant deficits in several behavioural tests, including rotarod, balance beam and gripping force tests (Extended Data Fig. 9f–h). Intraperitoneal injection of 10O5 or AN2, but not of DMSO only, significantly improved HD-relevant behavioural deficits in these tests, without influencing the wild-type mice (Fig. 5d–f), demonstrating a rescue of HD-relevant phenotypes. This is a proof-of-principle study, and further investigations will be required to establish the suitability for therapeutic application.

Discussion

We have identified mHTT–LC3 linker compounds that are able to reduce mHTT levels at nanomolar concentrations in HD cells and at 0.5 mg kg^{-1} by intraperitoneal injection in vivo (Extended Data Table 1). The compounds did not influence wtHTT, which has essential functions—especially during development and young adulthood[36]. These features of the compounds are highly desirable for the treatment of HD and potentially for the treatment of other polyQ diseases (Extended Data Fig. 9a–e), although preclinical studies of longitudinal efficacy and safety will be necessary for therapeutic development.

From a broader perspective, we have demonstrated the concept of using small-molecule compounds to target proteins (for example, mHTT) for autophagic degradation by linking them to LC3 (Fig. 5g). We selected mHTT as the target protein because wtHTT provides a good internal control for screening. We identified compounds that interact with both LC3B and mHTT; however, if no such compounds had been

identified, linker compounds could still be generated by conjugating a mHTT-interacting compound and an LC3-interacting compound using the nucleophile-isocyanate reaction used to create the SMMs. The critical next step in developing this concept will be to resolve the core chemical moiety that interacts with LC3 without influencing its function. Comprehensive medicinal chemistry and structural studies are needed to resolve the compound–LC3 interaction interface, which could then be developed to create a general degradation-targeting tool for conjugation with other compounds that interact with specific proteins of interest.

In summary, we have identified mHTT–LC3 linker compounds that are capable of lowering mHTT levels in vivo in an allele-selective manner and demonstrated the possibility of targeting proteins for degradation using autophagosome-tethering compounds, providing new entry points for drug discovery.

Online content

Any methods, additional references, Nature Research reporting summaries, source data, extended data, Supplementary Information, acknowledgements, peer review information; details of author contributions and competing interests; and statements of data and code availability are available at https://doi.org/10.1038/s41586-019-1722-1.

1. Kabeya, Y. et al. LC3, a mammalian homologue of yeast Apg8p, is localized in autophagosome membranes after processing. *EMBO J.* **19**, 5720–5728 (2000).
2. Scherzinger, E. et al. Huntingtin-encoded polyglutamine expansions form amyloid-like protein aggregates in vitro and in vivo. *Cell* **90**, 549–558 (1997).
3. Warrick, J. M. et al. Expanded polyglutamine protein forms nuclear inclusions and causes neural degeneration in *Drosophila*. *Cell* **93**, 939–949 (1998).
4. Fire, A. et al. Potent and specific genetic interference by double-stranded RNA in *Caenorhabditis elegans*. *Nature* **391**, 806–811 (1998).
5. Mali, P. et al. RNA-guided human genome engineering via Cas9. *Science* **339**, 823–826 (2013).
6. Cong, L. et al. Multiplex genome engineering using CRISPR/Cas systems. *Science* **339**, 819–823 (2013).
7. Winter, G. E. et al. Phthalimide conjugation as a strategy for in vivo target protein degradation. *Science* **348**, 1376–1381 (2015).
8. Lu, K., den Brave, F. & Jentsch, S. Pathway choice between proteasomal and autophagic degradation. *Autophagy* **13**, 1799–1800 (2017).
9. Mizushima, N., Levine, B., Cuervo, A. M. & Klionsky, D. J. Autophagy fights disease through cellular self-digestion. *Nature* **451**, 1069–1075 (2008).
10. Zhu, C. et al. Developing an efficient and general strategy for immobilization of small molecules onto microarrays using isocyanate chemistry. *Sensors* **16**, E378 (2016).
11. Fei, Y. et al. Screening small-molecule compound microarrays for protein ligands without fluorescence labeling with a high-throughput scanning microscope. *J. Biomed. Opt.* **15**, 016018 (2010).
12. Mangiarini, L. et al. Exon 1 of the HD gene with an expanded CAG repeat is sufficient to cause a progressive neurological phenotype in transgenic mice. *Cell* **87**, 493–506 (1996).
13. Liu, H. et al. Nuclear cGAS suppresses DNA repair and promotes tumorigenesis. *Nature* **563**, 131–136 (2018).
14. Landry, J. P. et al. Discovering small molecule ligands of vascular endothelial growth factor that block VEGF–KDR binding using label-free microarray-based assays. *Assay Drug Dev. Technol.* **11**, 326–332 (2013).
15. Fei, Y. et al. Characterization of receptor binding profiles of influenza A viruses using an ellipsometry-based label-free glycan microarray assay platform. *Biomolecules* **5**, 1480–1498 (2015).
16. Zhu, X. et al. Oblique-incidence reflectivity difference microscope for label-free high-throughput detection of biochemical reactions in a microarray format. *Appl. Opt.* **46**, 1890–1895 (2007).
17. Landry, J. P., Zhu, X. D. & Gregg, J. P. Label-free detection of microarrays of biomolecules by oblique-incidence reflectivity difference microscopy. *Opt. Lett.* **29**, 581–583 (2004).
18. Zhu, C. et al. Fast focal point correction in prism-coupled total internal reflection scanning imager using an electronically tunable lens. *Sensors* **18**, E524 (2018).
19. Menalled, L. B., Sison, J. D., Dragatsis, I., Zeitlin, S. & Chesselet, M. F. Time course of early motor and neuropathological anomalies in a knock-in mouse model of Huntington's disease with 140 CAG repeats. *J. Comp. Neurol.* **465**, 11–26 (2003).
20. Bondeson, D. P. et al. Catalytic in vivo protein knockdown by small-molecule PROTACs. *Nat. Chem. Biol.* **11**, 611–617 (2015).
21. Miller, J. et al. Identifying polyglutamine protein species in situ that best predict neurodegeneration. *Nat. Chem. Biol.* **7**, 925–934 (2011).
22. Fu, Y. et al. A toxic mutant huntingtin species is resistant to selective autophagy. *Nat. Chem. Biol.* **13**, 1152–1154 (2017).
23. Baldo, B. et al. TR-FRET-based duplex immunoassay reveals an inverse correlation of soluble and aggregated mutant huntingtin in Huntington's disease. *Chem. Biol.* **19**, 264–275 (2012).
24. Weiss, A. et al. Single-step detection of mutant huntingtin in animal and human tissues: a bioassay for Huntington's disease. *Anal. Biochem.* **395**, 8–15 (2009).
25. Lu, B. et al. Identification of NUB1 as a suppressor of mutant Huntington toxicity via enhanced protein clearance. *Nat. Neurosci.* **16**, 562–570 (2013).
26. Mizushima, N. et al. Dissection of autophagosome formation using Apg5-deficient mouse embryonic stem cells. *J. Cell Biol.* **152**, 657–668 (2001).
27. Lackey, K. et al. The discovery of potent cRaf1 kinase inhibitors. *Bioorg. Med. Chem. Lett.* **10**, 223–226 (2000).
28. Reddy, K. & D'Orazio, A. Highlights from the international conference on molecular targets and cancer therapeutics: discovery, biology, and clinical applications, Philadelphia, PA. ECCO 13–The European Cancer Conference, Paris, France, October 30-November 3, 2005. *Clin. Genitourin. Cancer* **4**, 156–159 (2005).
29. Johnson, G. L. & Lapadat, R. Mitogen-activated protein kinase pathways mediated by ERK, JNK, and p38 protein kinases. *Science* **298**, 1911–1912 (2002).
30. Tao, W. et al. An inhibitor of the kinesin spindle protein activates the intrinsic apoptotic pathway independently of p53 and de novo protein synthesis. *Mol. Cell. Biol.* **27**, 689–698 (2007).
31. Trettel, F. et al. Dominant phenotypes produced by the *HD* mutation in ST*Hdh*^{Q111} striatal cells. *Hum. Mol. Genet.* **9**, 2799–2809 (2000).
32. Kimura, S., Noda, T. & Yoshimori, T. Dissection of the autophagosome maturation process by a novel reporter protein, tandem fluorescent-tagged LC3. *Autophagy* **3**, 452–460 (2007).
33. Zhang, J., Wang, J., Ng, S., Lin, Q. & Shen, H. M. Development of a novel method for quantification of autophagic protein degradation by AHA labeling. *Autophagy* **10**, 901–912 (2014).
34. Ni, H. M. et al. Dissecting the dynamic turnover of GFP–LC3 in the autolysosome. *Autophagy* **7**, 188–204 (2011).
35. Feng, X., Luo, S. & Lu, B. Conformation polymorphism of polyglutamine proteins. *Trends Biochem. Sci.* **43**, 424–435 (2018).
36. Wang, G., Liu, X., Gaertig, M. A., Li, S. & Li, X. J. Ablation of huntingtin in adult neurons is nondeleterious but its depletion in young mice causes acute pancreatitis. *Proc. Natl Acad. Sci. USA* **113**, 3359–3364 (2016).
37. Vijayvargia, R. et al. Huntingtin's spherical solenoid structure enables polyglutamine tract-dependent modulation of its structure and function. *eLife* **5**, e11184 (2016).

Methods

Additional details from figure legends

In Fig. 5a, loss of processes and shrinkage of neurons were observed in HD neurons after BDNF removal. Bar plots show quantification of the area showing TUBB3 signal (TUBB3 area) normalized to the nuclei counts based on DAPI staining. The lower TUBB3 area per cell reflects neuronal processes shrinkage and loss. Data were normalized to the average of wild-type controls. The data were analysed by one-way ANOVA ($F(5, 60) = 94.78$) with post hoc Dunnett's tests. ****$P < 0.0001$; *n* indicates the number of independently plated wells.

Figure 5b, the images were captured every 3 h inside the incubator using Incucyte, and the caspase-3 active cells were quantified by the fluorescent-object count per field. The data were analysed by two-way ANOVA ($F(43, 516) = 12.85$) with post hoc Dunnett's tests, comparing to the HD_DMSO group. ****$P < 0.0001$. The numbers in brackets indicate the number of independently plated wells, with four fields per well imaged and averaged for quantification. Three batches were tested and showed consistent results.

In Fig. 5c, left, *Drosophila* expressed full-length HTT proteins (Q128 or Q16) in the nervous system driven by *elav-GAL4*. Seventy-five flies were tested for each group. The data were analysed by log-rank (Mantel–Cox) test, comparing compound-treated groups with DMSO controls in Q128 flies. ****$P < 0.0001$. Figure 5c, right, similar to Fig. 5c, left, but plotting the climbing performance as a function of age after eclosion. Data were analysed by two-way ANOVA ($F(4, 275) = 122.1$) with post hoc Dunnett's tests, comparing the compound treated groups with the DMSO controls in Q128 flies. Numbers in brackets indicate the number of vials (each containing 15 flies) tested. ****$P < 0.0001$.

In Fig. 5d–f, the numbers in brackets indicate the number of mice tested. The data were analysed by two-way ANOVA with post hoc Dunnett's tests, and *P* values were calculated for the comparison with the DMSO control. ****$P < 0.0001$. For HD mice, $F(2, 195) = 4.963$ in rotarod tests, $F(2, 195) = 37.31$ in balance beam tests, and $F(2, 156) = 7.068$ in gripping force tests. No significant difference was detected among wild-type mice injected with the different compounds. Investigators were blinded to the compounds and genotypes when performing the experiments. In all panels, graphical data are presented as mean and s.e.m.

Compound stamping on the microarray

SMMs containing 3,375 bioactive compounds were used for high-throughput screening of target proteins. The compound library containing 1,527 drugs approved by Food and Drug Administration (FDA) of United States, 1,053 natural products from traditional Chinese medicine, and 795 known inhibitors were stamped onto the SMMs. Each compound was dissolved in DMSO at a concentration of 10 mM and printed in duplicates along vertical direction on homemade phenyl-isocyanate functionalized glass slides with a contact microarray printer (SmartArrayer 136, CapitalBio Corporation). Biotin-BSA at a concentration of 7,600 nM in 1× phosphate-buffered saline (PBS) and biotin-$(PEG)_2$-NH_2 at a concentration of 5 mM in DMSO were printed as the inner and outer borders of SMMs, respectively. The diameter of each spot was about 150 μm and spacing between two adjacent spots was 250 μm. The printed SMMs were then dried at 45 °C for 24 h to facilitate covalent bonding of nucleophilic groups of small molecules to isocyanate groups of the functionalized slides. Afterwards, the SMMs were stored in a −20 °C freezer.

Expression and purification of recombinant proteins

The human microtubule-associated protein 1 light chain 3-β (*MAP1LC3B* (LC3B)) gene (GenBank: NM_022818.4) was amplified by PCR and cloned into a pGEX-6P1 (GE Healthcare) derived vector pGHT, which is a prokaryotic expression vector reconstructed by adding a His_8 tag and a TEV protease cleavage site before the pGEX-6P1 multiple cloning site. After sequencing verification, the expression plasmid pGHT-LC3B was introduced into *Escherichia coli* BL21 (DE3) pLsyS, in which the recombinant GST–LC3B protein was expressed by induction with IPTG. When the bacterial culture reached $OD_{600} = 0.8$, its temperature was decreased to 18 °C, and 0.2 mM IPTG was added into the culture for an additional 20 h incubation. The cells were then harvested by centrifugation (6,000*g*, 4 °C, 15 min) and the cell pellet was suspended in 50 mM Tris-HCl buffer, pH 7.5, with 150 mM NaCl and 5% glycerol. Cells were then disrupted by sonication, followed by centrifugation (20,000*g*, 4 °C, 60 min). The supernatants were then loaded onto a HisTrap HP column (GE Healthcare, cat. no. 17524701), and eluted with 50 mM Tris-HCl buffer, pH 7.5, containing 150 mM NaCl, 5% glycerol and 300 mM imidazole. The LC3B eluate was then mixed with TEV protease (Sigma, cat. no. T4455; eluted protein: TEV protease = 100:1) and dialysed against the dialysate buffer (50 mM Tris-HCl buffer, pH 7.5, containing 100 mM NaCl) in 4 °C overnight. After TEV protease treatment, the samples were then loaded onto a HisTrap HP column again, the flow through fraction which mainly contains tag removed recombinant LC3B. Afterwards, the proteins were concentrated and further purified by Superose 6 Increase 10/300 GL (GE Healthcare) size-exclusion chromatography. Finally, the purified proteins were concentrated to approximately 10 mg ml^{-1} in 50 mM HEPES buffer with 100 mM NaCl for further analysis. The MBP–His_8 and Rpn10 proteins were purified similarly.

The full-length HTT proteins, HTTexon1–MBP, polyQ–sfGFP and sfGFP were purified from mammalian cells. For full-length HTT proteins, the human *HTT* gene (GenBank: NM_002111.8) with $(CAG)_{23}$ or $(CAG)_{73}$ (23Q or 73Q for proteins) were de novo synthesized (by Genewiz), sequence validated and then cloned into a modified pCAG vector with an N-terminal protein A tag. The plasmid was transfected to human embryonic kidney E293 cells using polyethylenimine (PEI, from Polysciences, cat. no. 23966). After culture at 37 °C for 48 to 60 h, cells were collected and lysed at 4 °C for 1 h in lysis buffer containing 50 mM Tris-HCl, pH 8.0, 150 mM NaCl, 5% glycerol, 0.5% CHAPS, 3 mM DTT, 1% PMSF, 1 μg ml^{-1} pepstatin, 1 μg ml^{-1} leupeptin and 1 μg ml^{-1} aprotinin, 5 mM ATP and 5 mM $MgCl_2$. After centrifugation at 15,000 r.p.m. for 40 min, the supernatants were then incubated with IgG monoclonal antibody-agarose (Smart-lifesciences, cat. no. SA030010) for 2 h and unbound proteins were extensively washed away. The HTT proteins were then digested using TEV protease overnight to remove the protein A tag and eluted protein was further purified by ion exchange and gel filtration chromatography using Mono Q and Superose 6 (5/150 GL) columns from GE healthcare. The peak fractions were pooled for further biochemical analysis. The HTTexon1 with 25Q or 72Q cDNA were also de novo synthesized and cloned into a mammalian expression vector pTT5SH8Q2 for large scale production in HEK293T cells. In order to improve the production yield and increase the solubility, a C-terminal MBP tag was added after the HTTexon1 sequences to generate the pTT-HTTexon125Q-MBP and pTT-HTTexon125Q-MBP plasmids. For protein production and purification, the HEK293T cells were transfected by pTT-HTT25QExon1-MBP and pTT-HTT72QExon1-MBP plasmids with linear PEI (PolySciences cat. no. 24765), and then collected after 48 h. The cells were then lysed by sonication in buffer containing 50 mM Tris-HCl, pH 7.5, 150 mM NaCl, 20 mM imidazole, 5% glycerol, protease inhibitor cocktail (Sigma) and 50 U ml^{-1} benzonase (Sigma). After centrifugation, the supernatants were loaded onto HisTrap HP column (GE Healthcare), and eluted with the buffer containing 50 mM Tris-HCl, pH 7.5, 150 mM NaCl, 300 mM imidazole, 5% glycerol and protease inhibitor cocktail. The MBP tag was not cleaved to avoid precipitation. Afterwards, the proteins were concentrated and further purified by Superose 6 Increase 10/300 GL (GE Healthcare) size-exclusion chromatography.

Verifications of the recombinant proteins by MALDI–TOF

The purified LC3B, HTTexon1Q25–MBP, and HTTexon1Q72–MBP proteins were dialysed into 5 mM NH_4Ac by Superose 6 Increase size-exclusion chromatography for linear mode matrix assisted laser desorption

ionization-time of flight mass spectrometry (MALDI–TOF) analysis on a Bruker FLEX MALDI–TOF instrument. A total of 1,500–2,500 scans were averaged for each spectrum using an accelerating voltage of 25 kV. Sinapinic acid (SA, Bruker, cat. no. 820135) was used as the matrices for protein and peptide analyses. Sinapinic acid was made into 20 mg ml^{-1} solutions in 70% acetonitrile, 0.1% trifluoroacetic acid. For the acquisition of spectra from 10,000 to 100,000 amu, 2 µl of sample was mixed with 2 µl of sinapinic acid solution in an Eppendorf tube, and 2 µl of the mixture was loaded onto the MALDI plate. The calibration peptides for this range were BSA (M + 66,431) (Sigma, cat. no. A1933). All spectra were obtained in positive linear mode. The amount of full-length HTT proteins were limited, and thus not validated by MALDI–TOF. Instead, they were further purified by ion exchange and gel filtration chromatography, and validated by Coomassie blue staining (Extended Data Fig. 1e) and western blot (Fig. 4b).

Verifications of the recombinant LC3B by X-ray diffraction crystallography

Because the deletion of G120 (lipidation site) stabilizes LC3B protein, we used LC3B(ΔG120) protein to obtain high-resolution diffraction data. Purified LC3B(ΔG120) protein was concentrated in 20 mM HEPES pH 7.5, 150 mM NaCl. The LC3B(ΔG120) crystal was grown in reservoir solutions consisting of 0.16 M ammonium sulfate, 0.08 M sodium acetate pH 4.6, 20% (w/v) PEG4000, 20% (v/v) glycerol and 0.01 M taurine.

Refinement

The X-ray diffraction data were collected at 100 K in the beamline BL17U1 and BL19U1, SSRF. The wavelength for data collection was 0.97892 Å. Diffraction images were indexed and processed by HKL2000. The structure of LC3B(ΔG120) (PDB ID: 6J04, 1.90Å) was solved by molecular replacement with the Phaser 2.8 program from the CCP4 crystallography package using PDB structure 1UGM as the search model. The refinement was performed by Refmac 5.5 and Phenix 1.14. There are no Ramachandran outliers to report. The related figure was drawn using PyMOL 2.2.

Compound–protein interaction measurements by OI-RD

For high-throughput preliminary screening of target proteins, a SMM was assembled into a fluidic cartridge and washed in situ with a flow of 1× PBS to remove excess unbound small molecules. After washing, the SMM was scanned with a label-free OI-RD scanning microscope to image small molecules immobilized on glass slides. After it was blocked with 7,600 nM BSA in 1× PBS for 30 min, SMM was incubated with the target protein for 2 h. HTTexon1(Q25)–MBP at a concentration of 454 nM, HTTexon1(Q72)–MBP at a concentration of 238 nM, and LC3B at a concentration of 680 nM were screened on separate fresh SMMs. OI-RD images were scanned for each operation, including washing, blocking and incubation. The OI-RD difference images (images after incubation − images before incubation) were used for analysis, and vertical bright doublet spots indicated compounds that bind with target proteins in both replicates. Compounds 8F20 and 10O5 were identified to bind to HTTexon1(Q72)–MBP and LC3B, but not to HTTexon1(Q25)–MBP. The binding was further confirmed by kinetics measurements.

To measure binding kinetics of target proteins with compounds, we prepared new SMMs consisting of 8F20, 10O5 and AN2. Six identical microarrays were printed on one glass slide and each compound was printed in triplicates in a single microarray. The printed small SMMs were assembled into a fluidic cartridge with each microarray housed in a separate chamber. Before the binding reaction, the slide was washed in situ with a flow of 1× PBS to remove excess unbound samples, followed by blocking with 7,600 nM BSA in 1× PBS for 30 min. For binding kinetics measurement, 1× PBS was first flowed through a reaction chamber at a flow rate of 0.01 ml min^{-1} for 5 min to acquire the baseline. 1× PBS was then quickly replaced with the probe solution of the target protein at a flow rate of 2 ml min^{-1} for 9 s followed by a reduced flow rate at 0.01 ml min^{-1} to have the microarray incubated in the probe solution under the flow condition for 35 min (association phase of the reaction). The probe solution was then quickly replaced with 1× PBS at a flow rate of 2 ml min^{-1} for 9 s followed by a reduced flow rate of 0.01 ml min^{-1} to allow dissociation of probe for 30 min (dissociation phase of the reaction). By repeating the binding reactions of the target protein at three different concentrations on separate fresh microarrays, binding curves of compounds with the target protein at three concentrations were recorded with scanning OI-RD microscope. Reaction kinetic rate constants were extracted by fitting the binding curves globally using 1-to-1 Langmuir reaction mode.

Compound–protein interaction measurements by MST

The purified recombinant proteins were dialysed into 1× PBS, and then labelled according to the protocol of Protein labelling kit RED-NHS (Nanotemper, cat. no. L001). All the tested stock compounds (10 mM) dissolved in DMSO were also diluted into the same buffer for the final MST assay. The MST experiment was performed using Monolith NT.115 instrument (NanoTemper Technologies). Labelled proteins (500 nM) were mixed with the indicated concentrations of candidate compounds in reaction buffer containing 20 mM HEPES, pH 7.4, 150 mM NaCl. The MST data were then collected under 40% infrared laser power and 20% light-emitting diode power. The data were analysed by Nanotemper analysis software (v.1.5.41) and the K_d was determined.

cDNA plasmids for transfection in mammalian cells

The pEX-GFP-hLC3WT plasmid was obtained from Addgene (24987) to express LC3B. The pTT-HTTexon1-Q72-MBP-His and pTT-HTTexon1-Q25-MBP-His were generated by subcloning HTTexon1 cDNAs into the mammalian expression vector pTT-MBP-His and then transiently transfected into HeLa cells to express HTTexon1 proteins for the colocalization experiments. The polyQ-GFP sequences (expressing Met-polyQ-sfGFP) were de novo synthesized and subcloned into the pcDNA vector. All plasmids were sequence validated. For transient transfections, the cells were plated at 50% confluence. After 24 h, the cDNAs were transfected with Lipofectamine 2000 (Thermo Fisher Scientific, cat. no. 11668019) using the forward transfection protocol provided by the manufacturer.

Cell culture

For mouse primary cortical neuron cultures, cortices were isolated from postnatal day 0 pups following genotyping. Cortices were dissected into cold Ca^{2+}- and Mg^{2+}-free PBS buffer. Chopped small pieces were digested in solution containing 2.5% trypsin (Sigma, cat. no. P1005) and DNase I (0.1 mg ml^{-1}, Sigma, cat. no. D5025), for 20–30 min at 37 °C. Tissues were transferred to 10% FBS containing DMEM (Thermo Fisher Scientific, cat. no. 11965) to cease digestion. Neurons were then dissociated by trituration with fire-polished glass pipettes, collected by spinning and plated onto polylysine-coated dishes at 4×10^5 cells per 35-mm dish. The growth medium was composed of Neurobasal A medium (Thermo Fisher Scientific, cat. no. 10888022) with 1× B-27 (Thermo Fisher Scientific, cat. no. 17504044) and 1× N2 supplement (Thermo Fisher Scientific, cat. no. 17504048). Cytosine-arabinofuranoside (Sigma, cat. no. C1768) was added at 6 µM to inhibit glial growth.

Some of the primary patient fibroblasts were obtained from HD patients (Q47, Q49, Q55) and healthy sibling (WT, Q19) controls in a family with HD from Mongolia. The HD Q68 fibroblast line was obtained from Coriell Cell Repositories. The PD line was obtained from an idiopathic Parkinson's disease patient, and the SCA3 line was obtained from a patient with SCA3 harbouring the ATXN3 expansion mutation (Q74). The studies were approved by The Ethic Community of Institutes of Biomedical Sciences at Fudan University (#28) for obtaining the HD and wild-type patient fibroblasts, and by Huashan Hospital Institutional Review Board at Fudan University (#174) for obtaining the PD and fibroblasts from patients with SCA3. Verbal and written consent was

obtained from patients. The procedures were in compliance with all relevant ethical regulations. The immortalized fibroblasts were generated by infection of lentivirus expressing SV40T. For generation of iPS cells, the primary fibroblasts were transduced with the retroviral STEMCCA polycistronic reprogramming system (Millipore, cat. no. SCR548). The iPS cells were confirmed positive for Tra-1-81, Tra-1-60, SSEA-4 and Nanog by immunofluorescence and flow cytometry. All four vector-encoded transgenes were found to be silenced and the karyotype was normal. iPS cells were cultured in E8 medium (Thermo Fisher Scientific, cat. no. A1517001) on Matrigel (Corning, cat. no. 354277) surface. iPS cells were differentiated to Pax6-expressing primitive neuroepithelia (NE) for 10–12 days in a neural induction medium. Sonic hedgehog (SHH, 200 ng ml^{-1}) was added on days 10–25 to induce ventral progenitors. For neuronal differentiation, neural progenitor clusters were dissociated and placed onto poly-ornithine/laminin-coated coverslips at day 26 in Neurobasal medium (Thermo Fisher Scientific, cat. no. 21103049), with 1× B-27 (Thermo Fisher Scientific, cat. no. 17504044), 1× N-2 (Thermo Fisher Scientific, cat. no. 17504048), brain derived neurotrophic factor (BDNF, 20 ng/ml, Protech, cat. no. 450-02), glial-derived neurotrophic factor (GDNF, 10 ng/ml, Protech, cat. no. 450-10), insulin-like growth factor 1 (IGF1, 10 ng/ml, Protech, cat. no. 100-11) and Vitamin C (Sigma cat. no. D-0260, 200 ng/ml). The mouse striatal cells (STHdh) were obtained from Coriell Cell Repositories. The HEK293T cells and the HeLa cells were originally obtained from American Type Culture Collection (ATCC). STHdh, HeLa and HEK293T cells were cultured in DMEM (Thermo Fisher Scientific, cat. no. 11965) with 10% (vol/vol) FBS (Thermo Fisher Scientific, cat. no. 10082-147). Atg5 WT and KO MEFs were from N. Mizushima. All the mammalian cell lines were maintained at 37 °C incubator with 5% CO_2, except STHdh cells, which were maintained at 33 °C with 5% CO_2. The cells were tested every two months by a TransDetect PCR Mycroplasma Detection Kit (Transgen Biotech, cat. no. FM311-01) to ensure that they are mycoplasma free. The CellTiter-glo assay was performed to measure cell viability with the indicated compound treatment (Extended Data Fig. 2e) following the protocol provided in the kit (Promega, cat. no. G7570).

HD *Drosophila* models

The nervous system driver line *elav-GAL4 (c155)*, and the HTT-expressing lines *UAS-flHTT-Q16* and the *UAS-flHTT-Q128* (expressing human full-length HTT with 16Q and 128Q, respectively, when crossed to the GAL4 line) lines were obtained from the Bloomington *Drosophila* Stock Center at University of Indiana (http://flystocks.bio.indiana.edu/), and maintained in a 25 °C incubator. Crosses were set up between virgin female flies carrying *elav-GAL4* driver and the *UAS-flHTT-Q16* or *UAS-flHTT-Q128* male flies to generate the desired genotypes.

HD mouse models

The generation and characterization of the Hdh140Q knock-in mice have been previously described[19]. Mice were group-housed (up to 5 adult mice per cage) in individually vented cages with a 12 h light/dark cycle. The mouse experiments were carried out following the ARRIVE (Animal Research: Reporting of In vivo Experiments) guidelines, and they were in compliance with all relevant ethical regulations. The Animal Care and Use Committee of the School of Medicine at Fudan University approved the protocol used in animal experiments (Approval 20140904 and 20170223-005).

Compound treatment in cells and animals

The compounds used in this study were all commercially available, and quality controlled by the vendors using NMR. 10O5: GW5074 (DC Chemicals; cat.no. DC8810); 8F20: ispinesib (Selleck; cat.no. S1452); AN1: 5-bromo-3-[(4-hydroxyphenyl)methylidene]-2,3-dihydro-1*H*-indol-2-one (Specs; cat. no. AN-655/15003575); AN2: 5,7-dihydroxy-4-phenylcoumarin (ChemDiv; cat.no. D715-2435); GSK923295 (Selleck, cat. no. S7090), BAY1217389 (Selleck, cat.no. S8215), PLX-4720 (Selleck, cat.no. S1152), Dabrafenib (Selleck, cat.no. S2807), Sorafenib Tosylate (Selleck, cat.no. S1040), rapamycin (Sigma-Aldrich, cat. no. R8781).

For compound treatment in the cells, the compounds were diluted in culture medium to 10× concentrations and added to the plated cells: for primary cultured neurons and iPS-cell-derived neurons, the compounds were added 5 days after plating; for patient fibroblasts and other cell lines, the compounds were added 1 day after plating. The cells were then collected 2 days later for measurement of HTT levels. For detection of HTT-LC3 colocalization, the cells were fixed 4 h after compound treatment. For caspase-3 activation detection, the cells were stressed (BDNF removal for iPS-cell-derived neurons) 1 day after compound treatment, and tested at the indicated time points.

For compound treatment in the *Drosophila*, flies were maintained in standard maize food at 25 °C. For drug feeding, maize media was heated to 45 °C until liquid and distributed into vials. Compounds were freshly prepared in DMSO and added to the media. New adult flies were transferred to vials with 400 µL the control (DMSO) or compound-containing food, which was changed every other day.

For compound treatment in mice using intracerebroventricular (icv) injection, the 3-month-old mice were anesthetized using a small animal anaesthesia machine (MSS-3, MSS International) by isoflurane (1.5% solution). We surgically implanted each mouse with a guide cannula directed towards the lateral ventricle. The coordinates for implantation were determined using "The Mouse Brain in Stereotaxic Coordinates" and the guide cannulas were placed at 0.6 mm posterior, 1.5 mm lateral (left), and 1.7 mm dorsal with respect to bregma. A cap with stylus was then inserted into the guide cannula to seal its opening. Mice were then allowed to recover from surgery for a week before being treated. For injection, we first inserted an internal injector cannula so that it extended 0.5 mm beyond the tip of the guide cannula to reach the lateral ventricle. We then injected the mice through the internal injector cannula using a 25 µL syringe (Hamilton 1700 Series Microlitre Syringes, Bonaduz, GR, CH) at a flow rate of 0.25 µL/min powered by a syringe pump (KDS Legato 130) to administer 2 µL of compounds-containing artificial cerebrospinal fluid (ACSF: 1 mM glucose, 119 mM NaCl, 2.5 mM KCl, 1.3 mM $MgSO_4$, 2.5 mM $CaCl_2$, 26.2 mM $NaHCO_3$, 1 mM NaH_2PO_4) at a concentration of 25 µM (containing 0.125% vol/vol DMSO). 2 µL ACSF containing equivalent amount of DMSO (0.125% vol/vol) was used as the control. The injector cannula was left in place for approximately 60 s to allow for diffusion before placing the caps with stylus back in guide cannulas.

For compound treatment in mice using intraperitoneal (ip) injection, each mouse was weighed. The compounds were diluted with 0.9% NaCl intravenous infusion solution to 0.05 µg/µL (containing 0.011 µg/µL DMSO) and injected into each mouse based on the weight of the mouse (500 µg/kg, containing 110 µg/kg DMSO). As controls, equivalent amount of DMSO was diluted and injected in the same way. Injection of 0.9% NaCl intravenous infusion solution alone was also tested and showed no difference (Extended Data Fig. 9f–h). One injection per day was performed for two weeks before subsequent behavioural experiments or tissue extractions.

Note that in some of the experiments (Figs. 4, 5 and Extended Data Fig. 6b–d), 8F20 and/or AN1 were not tested. 8F20 was not tested because it did not have an effect in vivo by icv-injection (Extended Data Fig. 6a). AN1 was not tested because its structure is highly similar as 10O5 while it had a weaker HTT-lowering effect by icv-injection (Extended Data Fig. 6a).

Protein extraction from cells and tissues

For protein extraction from cells, the cell pellets were collected and lysed on ice for 30 min in 1× PBS + 1% Triton X-100 + 1× complete protease inhibitor (Sigma-Aldrich, cat. no. 11697498001), sonicated for 10 s, and spun at >20,000*g* at 4 °C for 15 min. The supernatants were then loaded and transferred onto nitrocellulose membranes for western blotting. For mouse brain tissues, the mouse striata and cortices were dissected

on ice and grinded by a tissue grinder for 5 min at 60 Hz and lysed on ice for 60 min in brain lysis buffer (50 mM Tris, 250 mM NaCl, 5 mM EDTA, 1% Triton X-100 PH7.4) + 1× complete protease inhibitor (Roche, cat. no. 4693159001). The samples were then sonicated for 10 cycles, 15 s on and 20 s off, and then collected for western blot.

For protein extraction from the mouse brain, the brains were collected and the cortices were acutely dissected on ice and homogenized with a tissue grinder for 5 min at 60 Hz and lysed on ice for 60 min in brain lysis buffer (50 mM Tris, 250 mM NaCl, 5 mM EDTA, 1% (vol/vol) Triton X-100, 1× complete protease inhibitor (Roche, cat. no. 4693159001), pH = 7.4). The samples were then sonicated for 10 cycles, 15 s on and 20 s off, and then collected for western blots, HTRF or dot blots.

For mHTT measurements in the HD *Drosophila* model, the fly heads were collected at the age of 7 days and lysed on ice for 30 min in PBS + 1% (vol/vol) Triton X-100 + 1× complete protease inhibitor (Roche, cat. no. 4693159001), sonicated for 10 cycles, 15 s on and 20 s off, and then collected for HTRF.

For all the samples, the protein concentrations were measured to correct the loadings. Different protein concentrations or cell numbers per well were tested to ensure that the signals were in the linear range. Background corrections were performed by subtracting the background signals from blank samples.

Western blot and filter trap assays

For western blots, the samples were loaded onto the SDS page gel (5–12% depending on the molecular weight of the protein of interest). The proteins on the gel were then transferred to the nitrocellulose membranes for blocking and antibody detection. The signal was detected with ECL (Bio-Rad, cat. no. 1705061) after 1 h incubation of the membrane with secondary antibody 1:10,000.

The filter trap assay was performed similarly as previously described[23], 2 µL (10 µg) aliquots of each sample were loaded onto nitrocellulose membranes stacked in the Bio-Dot microfiltration apparatus (Bio-Rad). The membrane was blocked for 1 h with 5% milk and incubated overnight with the antibody 4C9 at a concentration of 1.5 µg/µl in 5% milk diluted in PBS + 0.1% Tween-20. The signal was detected with ECL (Bio-Rad, cat. no. 1705061) after 1 h incubation of the membrane with secondary antibody 1:10,000.

HTRF assays

For HTRF, the assays were similar as previously described[25]. The cell or tissue lysates were diluted with the original lysis buffer PBS + 1% (vol/vol) Triton X-100 + 1× complete protease inhibitor (Roche), used for lysing the samples, and then detected with indicated antibody pairs diluted in the HTRF assay buffer (50 mM NaH_2PO_4, 400 mM NaF, 0.1% BSA, 0.05% (vol/vol) Tween-20, 1% (vol/vol) Triton X-100, pH 7.4). The donor antibody concentration was 0.023 ng/µL and the acceptor antibody concentration was 1.4 ng/µL, both in HTRF assay buffer. Different antibody pairs were used for different experiments as indicated in the figure legends. For all the samples, the signals were normalized to the total protein concentrations to ensure equal loadings. Different protein concentrations were pre-tested to ensure that the signals were in the linear range. Background corrections were performed by subtracting the background signals from blank samples.

In vitro c-Raf kinase assay

In vitro c-Raf kinase assays were carried out with a c-Raf kinase assay kit (BPS Bioscience, cat. no. 79570). The assays were performed in a 96-well plate according to the manufacturing instruction. The samples and non-reactive negative controls were tested in duplicate according to the instruction.

For details, 25 µL of the mixture containing 5× kinase assay buffer (6 µL), ATP (1 µL), 5× Raf substrate (10 µL) and water (8 µL) was added to a well. 5 µL of water solution containing a test compound at a 10× desired concentration (DMSO was at 10% at the water solution) was added to the 25 µL of mixture, and 20 µL of 1× kinase assay buffer containing 2 ng/µL c-Raf kinase was added to the mixture in a well to initiate the kinase reaction (at this stage compounds were at 1× desired concentration, and DMSO was at 1% concentration). For a non-reactive negative control, 20 µL of 1× kinase assay buffer containing no c-Raf was added to the mixture instead. The plate was incubated at 30 °C for 45 min. After the 45-min reaction, 50 µL of kinase Kinase-Glo Max reagent (Promega, cat. no. V6071) was added to each well, and the plate was incubated at room temperature for 15 min, in the dark. The plate was read with a microplate reader (BMG Labtech) for luminescence reading. The luminescence reading value measures the levels of ATP remaining, which is inversely related to kinase activity. The non-reactive negative control read value, indicating the level of initial added ATP, subtracted the level of ATP remaining (the luminescence reading) for the value of consumed ATP in the reaction that represents a kinase activity.

In vitro pull-down assays

We performed in vitro pull-down assays to test the compounds' influence on the HTT-LC3 interactions. The purified HTTexon1 (with the indicated tags), full-length proteins and the control proteins were incubated with amylose resin (New England BioLabs, cat. no. E8021L) at 4 °C for 30 min. Immobilized amylose resins were then washed three times with HBS (20 mM HEPES pH7.5, 150 mM NaCl, 0.05% Tween-20). The resulting amylose resins containing about 10 µg of MBP-fused proteins were incubated with the indicated compounds (1 µM for 10O5 and 100 nM for AN2) or the DMSO control at the same volume in 300 µl of HBS at 4 °C for 1 h using sample mixer. 40 µg of purified LC3B protein were then added and incubated at 4 °C for another 2 h using sample mixer. The resin-bound proteins were eluted with 40 µl maltose buffer (10 mM maltose, 20 mM HEPES, 150 mM NaCl, pH 7.5) and then added with 20 µl SDS–PAGE sample loading buffer. Samples were then analysed by SDS–PAGE and western blots.

GST pulldown was performed as the same procedures described above, except that GST-fused LC3B was immobilized onto magnetic conjugated GST mouse mAb beads (Cell Signaling Technology, cat. no.11847S) and eluted with SDS–PAGE protein loading buffer by vortex according to the instruction manual.

In Fig. 4a, b, for MBP pull-down (Fig. 4a), purified HTTexon1–MBP (10 µg) or MBP (10 µg) bound MBP resin were incubated with the purified LC3B protein (40 µg) and the indicated compounds. The HTTexon1–MBP or the MBP proteins were pulled down and the eluates were tested for co-precipitated LC3B. Four per cent of the total eluate was loaded in each lane, and the input:pull-down loading ratio was 100%. Both 10O5 and AN2 enhanced LC3B's interaction with HTTexon1-Q72–MBP, but not HTTexon1-Q25–MBP. Note that the MBP blot signals were much weaker for the Q72 protein, possibly because recognition of the MBP tag by the antibody was affected in the fusion protein. Meanwhile, data interpretation was not influenced, because compound treatments did not alter the MBP signals for the Q72 protein (last three lanes). The GST pull-down (Fig. 4b) was performed similarly, except using full-length HTT-Q73 or full-length HTT-Q23 (both without fusion tags) and GST–LC3B proteins for the in vitro GST pull-down experiments to precipitate GST–LC3B or GST alone with its binding proteins, and then eluted for detection. Note that the pull-down is in the reverse direction of the pull-down in (Fig. 4a). The input:pull-down loading ratio for the GST blot was 100%, whereas the ratio for the HTT blot was 10% to avoid overexposure of the input. Both 10O5 and AN2 enhanced LC3B's interaction with the full-length HTT-Q73 but not the full-length HTT-Q23 protein.

Imaging-based autophagy assays

Analysis of GFP-LC3 puncta for measuring autophagosomes: HeLa cells stably expressing GFP-LC3 were generated by transfection of pEGFP C1-LC3, and positive clones were selected by 500 µg/ml G418. The cells were then treated with vehicle (DMSO, 0.1%), 10O5, or AN2 for the indicated concentration, chloroquine (CQ, 20 µM) treatment was used as

a control. After 24 h, cells were fixed in 4% paraformaldehyde (PFA) for 10 min. Images were acquired with confocal microscopy (Leica SP8) by the observer blinded to the identity of the slides. The number and size of GFP vesicles per cell was determined by Image J software. Images were processed with the despeckle function to decrease the noise, and a threshold was set to highlight puncta. Cells were selected by the freehand drawing tool. The analyse-particle function was used for the sizes and numbers of GFP puncta.

The mRFP-GFP-LC3 assay: this assay allows us to monitor autophagosome synthesis and maturation/fusion by labelling autophagosomes (green and red) and autolysosomes (red), since the low lysosomal pH in autolysosomes quenches the GFP signals[32]. HeLa cells stably expressing mRFP-GFP-LC3[32] were treated with vehicle (DMSO, 0.1%), 10O5, or AN2 for the indicated concentration, bafA1 (10 nM) treatment was used as a control. After 24 h, cells were fixed in 4% PFA for 10 min. Images were acquired with confocal microscopy (Leica SP8) by the observer blinded to the identity of the slides. The green and red single channel images were analysed by Image J to quantify green and red puncta in the same way as in the GFP-LC3 assay described above.

In Fig. 4c, d, representative confocal microscopy images (scale bar, 10 μm) and quantifications of the co-localization between HTTexon1-MBP-His (red, detected by anti-His immunofluorescence) and LC3B–GFP (green, detected by GFP fluorescence directly) in transiently transfected HeLa cells (Fig. 4c) or between endogenous mHTT and LC3-II in the HD-knock-in mouse striatal cells ($STHdh^{Q111/Q111}$) (Fig. 4d). For overexpressed proteins (Fig. 4c), the cells transfected with LC3B–GFP alone or HTTexon1–MBP–His alone were imaged in both channels to ensure the specificity of the signals (top). The white arrows indicate representative co-localization puncta. Parts of the images have been magnified to show co-localization puncta more clearly (indicated by orange arrows). Since the puncta were obvious, co-localization was analysed by counting the red^+green^+ (yellow) and the total red^+ puncta directly, and then calculating the ratio for each cell. Blind analysis was performed for quantifications. For endogenous proteins (Fig. 4d), mHTT was detected by the anti-HTT antibody 2166, and the endogenous LC3-II was detected by an anti-LC3 antibody that has been reported to specifically detect LC3-II[32]. Since the signals of endogenous proteins were more dispersed, the co-localization analysis was performed blindly by measuring the red^+green^+ (yellow) and the total red^+ pixels using ImageJ, and then calculate the ratio for each cell.

Detection of long-lived proteins by click-chemistry

As an indicator of autophagy activity, the degradation of long-lived proteins was measured similarly as previously reported[33]. In brief, the HeLa cells with 70–80% confluency in a 6-well plate were washed with warm PBS and cultured in Met-free DMEM (Thermo Fisher Scientific, cat. no.21013) added with dialysed FBS for 1 h to deplete intracellular free Met reserves. The Met analogue L-AHA (50 μM) was then added to label the proteins for 18 h. After labelling, the cells were washed with PBS and cultured in regular culture medium containing 10× L-Met (2 mM) for 2 h to chase out short-lived proteins. The cells were then treated with the compounds versus the DMSO controls for 6 h before cell lysis and protein extraction. For the starvation sample, the culture medium was replaced with EBSS (Thermo Fisher Scientific, cat. no. 24010043) for 6 h. The protein lysates were then used for the click reaction by the Click-it reaction kit (Click Chemistry tools, cat. no. C1001) following manufacturer's instructions, and the remaining L-AHA containing long-lived proteins were then conjugated with biotin. These proteins were then analysed by electrophoresis and detected by the HRP-conjugated streptavidin (Beyotime, cat. no. A0303).

Immunofluorescence and caspase-3 imaging

For immunofluorescence of cultured cells, cells were fixed in 4% PFA for 10 min after washing with 1× PBS three times, and then washing and permeabilized in 0.5% (vol/vol) TritonX-100 for 10 min. The cells were then blocked in blocking buffer (4% BSA + 0.1% (vol/vol) Triton X-100 in 1× PBS) for 30 min and incubated overnight at 4 °C with primary antibodies, and then washed three times with blocking buffer and incubated with secondary antibody at room temperature for 1 h. Coverslips were then washed three times, stained with 0.5 mg/ml DAPI for 5 min at room temperature, and then mounted in vectashield mounting medium (Vector, cat.no. H-1002). Images were taken by Zeiss Axio Vert A1 confocal microscopes and analysed blindly by ImageJ for co-localization and TUBB3 quantifications. For co-localization experiments of transfected HeLa cells (Fig. 4c), the GFP signals were used to detect GFP-LC3B, and anti-His was used to detect HTTexon1-MBP-His proteins. Empty vector transfected cells were imaged to ensure the specificity of the signals. The co-localization was analysed by calculating the ratio between overlapping puncta and the HTT (red) puncta for each cell, and the puncta numbers were counted blindly. For co-localization experiments of $STHdh^{Q111/Q111}$ cells, the endogenous mHTT protein was stained with the HTT antibody (Millipore, cat. no. MAB2166), and autophagosomes were stained with the LC3B antibody (Thermo Fisher Scientific, cat. no. 700712), which preferentially detects LC3-II[38]. The co-localization was analysed by ImageJ to calculate the ratio between overlapping pixels and the HTT (red) positive pixels, because the signals of the endogenous proteins were more dispersed and could not be counted accurately. For TUBB3, the total area of TUBB3 signals and the DAPI counts were analysed by ImageJ. The former is then divided by the latter to calculate the averaged area of TUBB3 in each neuron as an index for neurodegeneration in vitro.

For caspase-3 activity measurements of the iPS-cell-derived neurons, the NucView 488 caspase-3 dye (Biotium, cat. no. 30029) was used for the caspase 3 activity detection as an indicator for apoptosis. The images were then taken every 3 h using the Incucyte technology (Essen Bioscience, IncuCyte FLR), which takes images of 4 different fields in each well inside the cell culture incubator. The quantification was performed by the Incucyte 2011A software, which identified the green fluorescent puncta and quantified the fluorescent object count per field. The 4 fields per well were quantified and averaged, and 4 independent wells were used for statistical analysis.

Antibodies

Antibodies used for western blots, HTRF and/or immunofluorescence/immunohistochemistry are as follows: the HTT antibodies 2B7[24], ab1[39] and MW1[40] have been described previously; commercially purchased antibodies include HTT antibody 2166 (Millipore, cat. no. MAB2166), anti-polyQ antibody 3B5H10 (Sigma, cat. no. P1874), anti-HTT antibody (D7F7)XP (Cell Signaling Technologies, cat. no. 5656 s), anti-β-tubulin (Abcam, cat. no. ab6046), anti-TUBB3 (Biolegends (previously Covance), cat. no. 801202), anti-ATXN3 (Millipore, cat. no. MAB5360); anti-Gapdh (Proteintech, cat. no. 60004-1), anti-NBR1 (Thermo Fisher Scientific, cat. no. PA5-54660), anti-β-actin (Beyotime, cat. no. AA128); anti-TBP (Abcam, cat. no. ab818); anti-P62 (Thermo Fisher Scientific, cat. no. PA5-27247); anti-spectrin (Millipore, cat. no. MAB1622); anti-Ncoa4 (Santa cruz, cat.no. sc-373739); anti-GST (ProteinTech, cat. no. HRP-66001); anti-GFP (Cell Signaling Technologies, cat. no. 2956); anti-MBP (ProteinTech, cat. no. 15089-1-AP); anti-His (Beyotime, cat. no. AH367); anti-BUBR1 (BD Transduction, cat.no, 612503); anti-phospho-p44/42 MAPK (ERK1/2) and anti-phospho-MEK1/2 in the Phospho-Erk1/2 Pathway Sampler Kit (Cell Signaling Technology, cat.no. 9911); anti-LC3B (Thermo Fisher Scientific, cat. no. PA1-16930 (for western blot) and cat. no. 700712 (for immunofluorescence)). All the antibodies used for immunofluorescence in this study have been validated by knock-down experiments. All the HTT, polyQ and ATXN3 antibodies used for HTRF and/or western blots have been validated by knock-down experiments and by comparing the signals from different genotypes in previous studies from us and others. All the other antibodies have been validated by previous literature or the vendor.

Compound detection in vivo in brain tissue from ip-injected mice

The experiments were performed by the SIM-Servier joint laboratory. The mice, ip-injected with DMSO or the indicated compounds, were anesthetized by chloral hydrate (200 µL/kg of 10% stock) at indicated time points, and the heart blood was collected by vacuum blood collection tubes. The heart blood samples were further spun at 10,000 r.p.m. for 5 min to generate the heart plasma. The mice were then perfused with 1× PBS to remove the blood. The mice were then euthanized and the brain samples were dissected. Five times the volume of methanol: acetonitrile (50: 50, vol/vol) were added to each sample, which was then homogenized. Following ultrasonic treatment for 15 min, the homogenates were centrifuged for 5 min, then 20 µL supernatant liquid was mixed with 20 µL water for 30 s before injection. Linear range of 10O5 was 10–30,000 ng/mL, and the linear range of AN2 was 0.3–10,000 ng/mL. The LC-MS/MS analyses were performed on an Acquity ultra performance liquid chromatography (UPLC) system (Waters Corporation) coupled to a Xevo TQ-S mass spectrometer (Waters Corporation). Chromatographic separation was performed using an Acquity UPLC BEH C18 (1.7 µm 2.1 × 50 mm) column supplied by Waters at a flow of 0.5 mL/min. Gradient elution was used with a mobile phase composed of solvent A (water containing 0.1% formic acid and 5 mM NH_4AC) and solvent B (acetonitrile: methanol (9:1,vol/vol) containing 0.1% formic acid).

Proteomics analysis

Samples were analysed on Orbitrap Fusion Lumos mass spectrometers (Thermo Fisher Scientific) coupled with an Easy-nLC 1000 nanoflow LC system (Thermo Fisher Scientific). Dried peptide samples were re-dissolved in Solvent A (0.1% formic acid in water) and loaded to a trap column (100 µm × 2 cm; particle size, 3 µm; pore size, 120 Å; SunChrom) with a max pressure of 280 bar using Solvent A, then separated on a 150 µm × 15 cm silica microcolumn (particle size, 1.9 µm; pore size, 120 Å; SunChrom) with a gradient of 5–35% mobile phase B (acetonitrile and 0.1% formic acid) at a flow rate of 600 nl min^{-1} for 75 min. The FAIMS device was placed before the mass spectrometer. FAIMS separation was performed with the following settings: inner electrode temperature = 100 °C, outer electrode temperature = 100 °C, carrier gas flow = 4.6 l min^{-1}, dispersion voltage = −5,000 V, entrance plate voltage = 250 V. The FAIMS carrier gas is N_2 only. The noted CVs were applied to the FAIMS electrodes. Each of the selected CVs was applied to sequential survey scans and MS/MS cycles (1 s); the MS/MS CV was always paired with the appropriate CV from the corresponding survey scan. For detection with Fusion or Fusion Lumos mass spectrometry, a precursor scan was carried out in the Orbitrap by scanning m/z 300–1400 with a resolution of 120,000. The most intense ions selected under top-speed mode were isolated in Quadrupole with a 1.6 m/z window and fragmented by higher energy collisional dissociation (HCD) with normalized collision energy of 30%, then measured in the linear ion trap using the rapid ion trap scan rate. Automatic gain control targets were 5×10^5 ions with a max injection time of 50 ms for full scans and 1×10^4 with 35 ms for MS/MS scans. Dynamic exclusion time was set at 18 s. Data were acquired using the Xcalibur software (Thermo Scientific).

Raw files were searched against the human National Center for Biotechnology Information (NCBI) Refseq protein database (updated on 04-07-2013, 32,015 entries) by Mascot 2.3 (Matrix Science) implemented on Proteome Discoverer 2.2 (Thermo Scientific). The mass tolerances were 20 ppm for precursor and 0.5 Da for product ions for Fusion Lumos. Up to two missed cleavages were allowed. The search engine set cysteine carbamidomethylation as a fixed modification and *N*-acetylation, oxidation of methionine as variable modifications. Precursor ion score charges were limited to +2, +3, and +4. The data were also searched against a decoy database so that protein identifications were accepted at a false discovery rate of 1%. Label-free protein quantifications were calculated using a label-free, intensity-based absolute quantification (iBAQ) approach.

Proteins with at least 2 unique peptides with 1% FDR at the peptide level and Mascot ion score greater than 20 were selected for further analysis. The file used for protein inference and protein FDR calculation was derived from Mascot search results, and the peptide spectrum match (PSM) was filtered via Percolator and customized parameters, and then the proteins were assembled. The protein FDR was calculated depending on the ratio of NPD (the number of assembled proteins from decoy database searches) and NPT (the number of assembled proteins from target database searches). The FOT was used to represent the normalized abundance of a particular protein across samples. FOT was defined as a protein's iBAQ divided by the total iBAQ of all identified proteins within one sample. The FOT was multiplied by 10^5 for the ease of presentation. Only the proteins detection in all compared samples were used for comparison.

Behavioural and lifespan experiments in HD *Drosophila* models

For behavioural experiments, we placed 15 age-matched virgin female flies in an empty vial and tapped them down. The percentage of flies that climbed past a 7-cm-high line after 15 s was recorded. The mean of five observations is plotted for each vial on each day, and data from multiple vials containing different batches of flies were plotted and analysed by two-way ANOVA tests. The flies were randomly placed into each tube. For lifespan measurements, we placed 75 age-matched virgin female flies in an empty plastic vial and recorded the survival situation for each vial on each day. For both behavioural and lifespan measurement experiments, the person who performed the experiments were blinded to the drugs fed until data analysis.

Behavioural experiments in HD mouse models

All the behavioural experiments were performed during the light phase and the experimenters were blinded to the compound treatment and the genotype of each mouse. Both males and females were used. All the mice were kept in the behavioural test room in dim red light for 1 h before starting the experiments. For rotarod experiments, mice were pre-trained on 3 consecutive days on the rotarod rotating at 4 r.p.m. for 2 min. Mice were then tested for five days at an accelerating speed ranging from 4 to 40 r.p.m. within 2 min. Each performance was recorded as the time in seconds spent on the rotating rod until falling off or until the end of the task. Each test included three repetitions with an inter-trial interval of 60 min in order to reduce stress and fatigue, and the means from these three runs were analysed for each mouse. The balance beam test was run using a 2-cm-thick metre stick suspended from a platform on both sides by metal grips. The total length is 100 cm. There was a bright light at the starting point and a dark box with food at the endpoint. The total time for each mouse to walk through the beam was recorded. For gripping force measurements, mice were allowed to grip the metal grids of a grip meter (Ametek Chatillon) with their forelimbs, and they were gently pulled backwards by the tail until they could no longer hold the grids. The peak grip strength observed in 10 trials was recorded.

Statistics

To ensure to reach a statistical power >0.8, power analyses were performed for each assay based on estimated values by PASS 16 (https://www.ncss.com/software/pass/) before experiments. Estimation was based on our previously published results on similar experiments and preliminary experiments. The effect size was also estimated by Cohen's d, two means divided by the standard deviation for the data. The power analysis suggested $n \geq 3$ for mHTT level measurements and $n \geq 5$ for behavioural experiments. In all the experiments we performed, we have used a larger n than these numbers in case the effect was smaller than preliminary results, and we also performed post-experiment power analyses to ensure that power ≥ 0.8 for all the significant differences. Statistical comparisons between two groups were conducted by the unpaired two-tailed t-tests. Statistical comparisons among multiple

groups were conducted by one-way ANOVA tests and post hoc tests for the indicated comparisons (Dunnett's tests for comparison with a single control, and Bonferroni's tests for comparisons among different groups). Statistical comparisons for series of data collected at different time points were conducted by two-way ANOVA tests. The similarity of variances between groups to be compared was tested when performing statistics in GraphPad Prism 7 and Microsoft Excel 2016. Normality of data sets was assumed for ANOVA and *t*-tests, and was tested by Shapiro–Wilk tests. When the data were significantly different from normal distribution, nonparametric tests were used for statistical analysis. All statistical tests were unpaired and two-tailed.

For the in vivo experiments in the mouse, randomization was performed by assigning random numbers. For the *Drosophila* experiments, the flies were randomly distributed into the vials after anesthesia.

Reporting summary

Further information on research design is available in the Nature Research Reporting Summary linked to this paper.

Data availability

The protein structure data has been uploaded to the Protein Data Bank with accession number 6J04. Source data for all figure plots are provided with the paper. The full gel blots and the proteomics data sets have been provided in the Supplementary Information. The data that support the findings of this study are available from the corresponding authors upon reasonable request.

38. Hancock, M. K., Hermanson, S. B. & Dolman, N. J. A quantitative TR-FRET plate reader immunoassay for measuring autophagy. *Autophagy* **8**, 1227–1244 (2012).
39. Sapp, E. et al. Native mutant huntingtin in human brain: evidence for prevalence of full-length monomer. *J. Biol. Chem.* **287**, 13487–13499 (2012).
40. Ko, J., Ou, S. & Patterson, P. H. New anti-huntingtin monoclonal antibodies: implications for huntingtin conformation and its binding proteins. *Brain Res. Bull.* **56**, 319–329 (2001).

Acknowledgements We thank J. Lu, M. Jiang, L. Liu and Q. Huang for their technical support with mouse behavioural experiments, Y. Xu for technical support with protein purification and H. Saiyin for help with obtaining human patient fibroblasts. We thank the following for funding support: National Key Research and Development Program of China (2016YFC0905100), National Natural Science Foundation of China (8192500069, 81870990, 31961130379, 91649105, 31470764, 91527305 and 61505032), Science and Technology Commission of Shanghai Municipality (18410722100), Natural Science Foundation of Shanghai (19ZR1405200), Shanghai Municipal Science and Technology Major Project (No.2018SHZDZX01), ZJLab and Hereditary Disease Foundation.

Author contributions B.L. conceived the idea, initiated the project, designed experiments, analysed data and wrote the manuscript. Y.F. and C.Z. performed the OI-RD screening and K_{on}/K_{off} measurements with data analysis. Y. Ding, Z.W., J.L. and C.G. performed protein purification, in vitro pull-down and structural biology experiments with data analysis. With help from others for blinding, Z.L. performed HTT measurements in cells and in mouse models, the mouse phenotype experiments, the autophagy-related mechanistic experiments, the control protein measurements and neurotoxicity measurements. C.W. replicated the HTT measurement and autophagy-related mechanistic experiments performed by Z.L. and performed additional HTT measurement and phenotypic experiments in HD fly models, patient iPS-cell-derived neurons and MEFs, as well as all measurements of other polyQ proteins and all the MST experiments. Y. Dang provided the compound library for the screen. T.S. and C.D. performed proteomics experiments and analysis. S.L. and Y.Y. performed the measurements of autophagy function. L.M., Y.S. and J.W. provided and characterized the patient cell lines. X.S. did the initial subcloning of full-length HTT and found the explanation for the observed 'hook effects'. C.L. performed biostatistical analysis. M.D. and Y.M. helped with designing the experiments and interpreting the data.

Competing interests B.L., Y.F., Y. Ding and Y. Dang have filed two patents together on the basis of this study to the State Intellectual Property Office of China (201910180674.7 and 201910180717.1).

Additional information

Supplementary information is available for this paper at https://doi.org/10.1038/s41586-019-1722-1.

Correspondence and requests for materials should be addressed to Y.D., Y.F. or B.L.

Peer review information *Nature* thanks David Rubinsztein, Huda Yahya Zoghbi and the other, anonymous, reviewer(s) for their contribution to the peer review of this work.

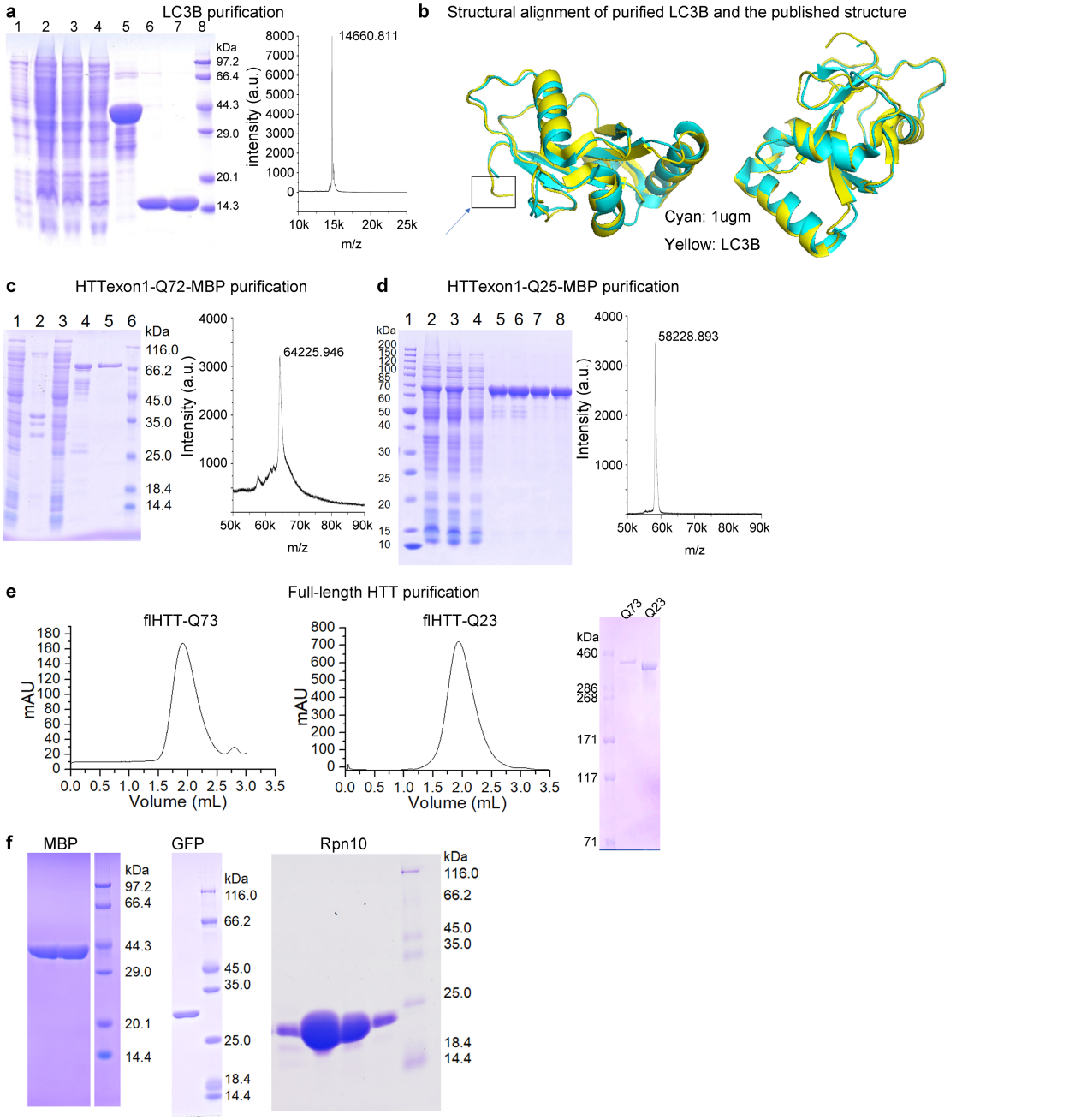

Extended Data Fig. 1 | Protein purifications. a, SDS–PAGE and linear mode MALDI–TOF mass spectrometry analysis of the expression and purification of recombinant LC3B protein. Left, SDS–PAGE: lane 1, the whole cell lysate before induction; lane 2, the whole cell lysate after induction; lane 3, the supernatants of induced cells; lane 4, the flow through fraction of Ni-NTA chromatography; lane 5, the eluates of Ni-NTA chromatography (GST–His_8–LC3); lane 6, LC3B eluate after removal of GST–His_8 tag by TEV protease; lane 7, the eluates of size-exclusion chromatography; lane 8, molecular weight marker. Right, *m/z* peak of recombinant LC3B is 14,660.811, consistent with theoretical calculations. **b**, Structural alignment of purified recombinant LC3B(ΔG120) (PDB ID: 6J04, yellow) with published LC3B structure (PDB ID: 1UGM, cyan) by PyMOL. **c**, **d**, SDS–PAGE and linear mode MALDI–TOF mass spectrometry analysis of the HTTexon1 proteins. **c**, Left, SDS–PAGE for HTTexon1(Q72)–MBP: lane 1, the supernatants of induced cells; lane 2, the insoluble fraction of induced cells; lane 3, the flow through fraction of Ni-NTA chromatography; lane 4, the eluates of Ni-NTA chromatography; lane 5, the eluates of size-exclusion chromatography; lane 6, molecular weight marker. **d**, Left, SDS–PAGE for HTTexon1(Q25)–MBP: lane 1, molecular weight marker; lane 2, the induced cell lysate; lane 3, the supernatant fraction of induced cells; lane 4, the flow-through fraction of Ni-NTA chromatography; lanes 5 and 6, the eluates of Ni-NTA chromatography; lanes 7 and 8, the eluates of size-exclusion chromatography. The *m/z* peaks of HTTexon1(Q72)–MBP (**c**, right) and HTTexon1(Q25)–MBP (**d**, right) are 64,225.946 and 58,228.893, consistent with theoretical calculations. **e**, Left and middle, size-exclusion chromatography of the recombinant full-length HTT(Q73) (flHTT–Q73) and HTT(Q23) (flHTT-Q23) proteins using Superose 6 5/150 GL. The major peak fractions were collected pooled together for the SDS–PAGE analysis (right). **f**, SDS–PAGE analysis of purified MBP–His_8 (MBP), sfGFP (GFP) and Rpn10 proteins.

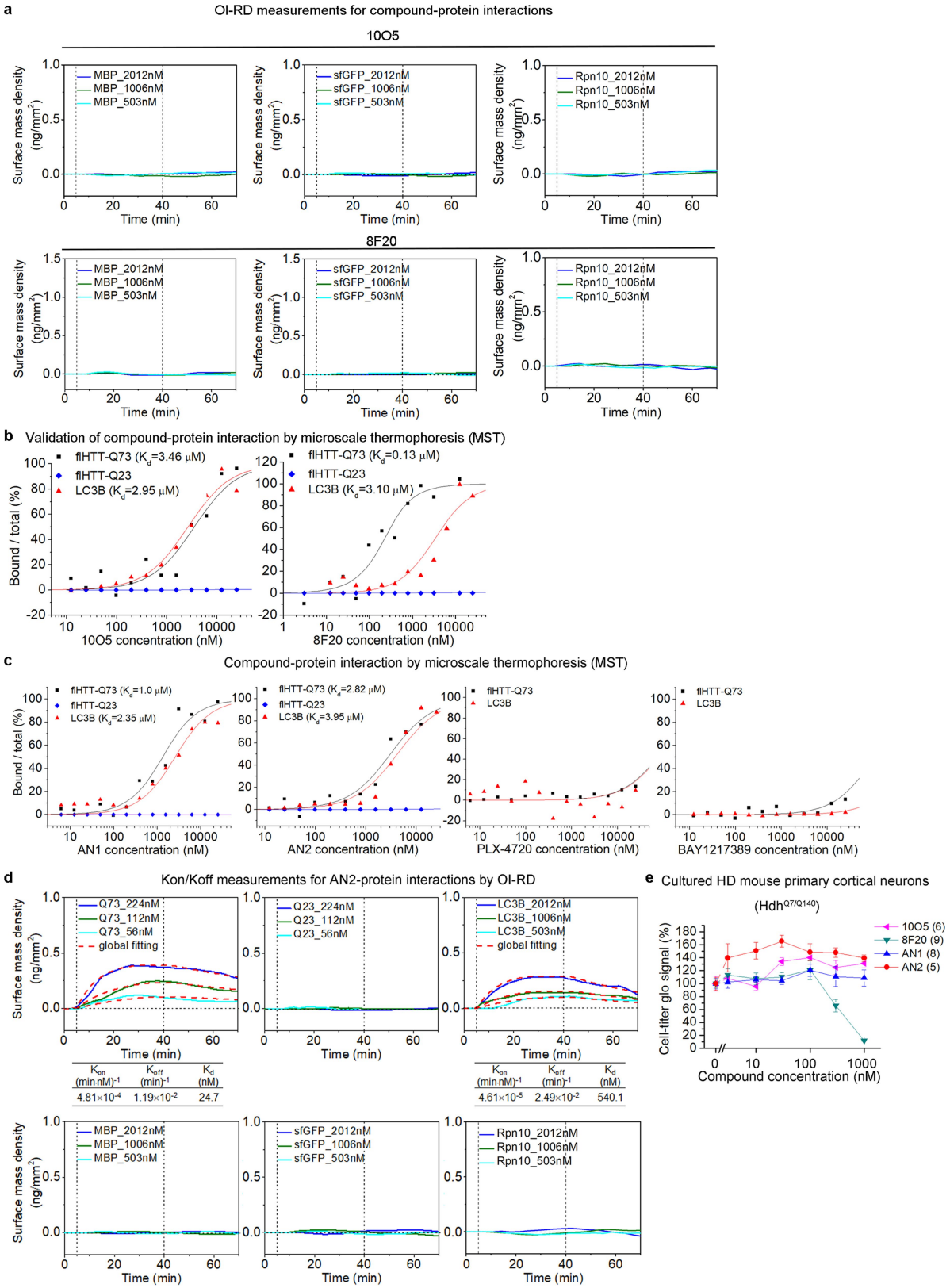

Extended Data Fig. 2 | See next page for caption.

Extended Data Fig. 2 | Negative controls for OI-RD measurements and validation of the compounds' interaction with HTT and LC3 by MST. **a**, Similar to Fig. 1c–e, but for negative control proteins MBP–His_8 (MBP), sfGFP and Rpn10 (Rpn10). Association–dissociation curves of surface immobilized compounds 8F20 and 10O5 with these proteins were measured by OI-RD, and no compound–protein interactions were detected. For all association–dissociation curves, vertical dashed lines mark the starts of association and dissociation phases of the binding event. **b**, Binding of 10O5 and 8F20 to full-length HTT(Q73) (flHTT(Q73), black dots) or LC3B (red dots) in standard treated capillaries measured by MST. The compound-bound protein fractions (bound/total) were calculated from the MST signals (F_{norm}) at each compound concentration, as well as the bound (F_{norm_bound}, set as 100%) and the unbound ($F_{norm\_unbound}$, set as 0%) MST signals: bound/total = (F_{norm} – $F_{norm\_unbound}$)/(F_{norm_bound} – $F_{norm\_unbound}$) × 100%. The fitted curves and K_d values calculated by Nanotemper analysis software (v.1.5.41) for flHTT(Q73) and LC3B are indicated in each panel. Consistent with the OI-RD measurements (Fig. 1e), no binding was observed for the flHTT(Q23) protein (blue dots). The MST experiments were repeated more than three times and showed consistent results. **c**, Similar to **b**, except using the compounds indicated on the *x* axis. MST measurements of the binding of indicated compounds to full-length HTT(Q73) (flHTT-Q73), full-length HTT(Q23) (flHTT-Q23) and LC3B in standard treated capillaries. The proteins tested are indicated in the legends. **d**, Similar to Fig. 1c–e, but plotting the association–dissociation curves of surface immobilized compound AN2 with full-length HTT(Q73) (Q73), or full-length HTT(Q23) (Q23), LC3B or the negative-control proteins MBP–His_8 (MBP), sfGFP and Rpn10. For all association–dissociation curves, vertical dashed lines mark the starts of association and dissociation phases of the binding event. The red dashed lines are global fits to a Langmuir reaction model with the global fitting parameters listed at the bottom of each plot. No binding signals were observed for full-length HTT(Q23) proteins, and thus the parameters were not presented. **e**, Cell viability measurement of cultured HD neurons measured by the CellTiter-glo assay. No toxicity was observed within the concentration range presented in Fig. 2, although the compound 8F20 became toxic to the cells when the concentration reached 300 nM.

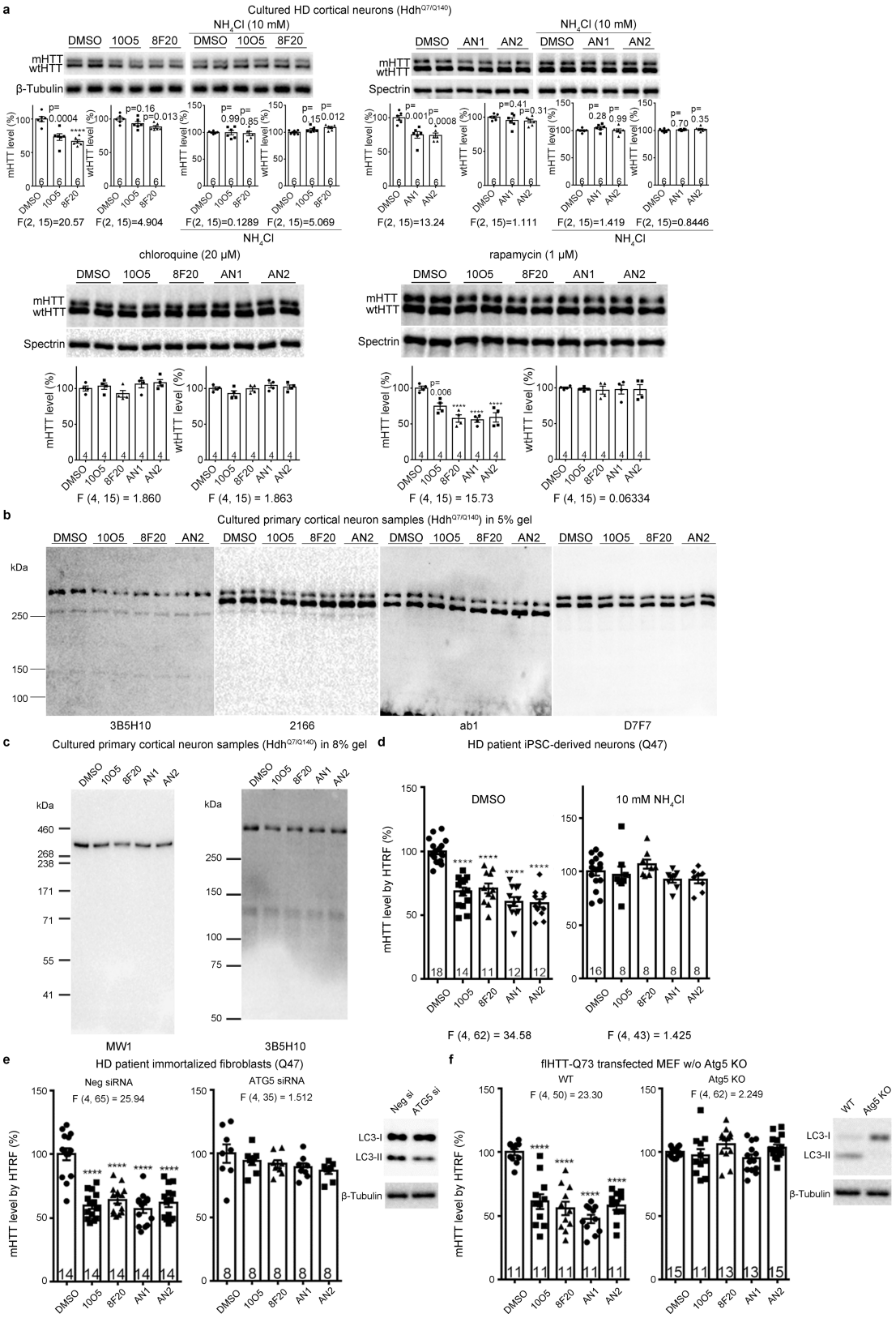

Extended Data Fig. 3 | See next page for caption.

Extended Data Fig. 3 | mHTT-lowering effects by mHTT-linker compounds could be detected by multiple antibodies and were dependent on autophagy. a, Representative western blots (HTT detected by the 2166 antibody) and quantifications of compound-treated cultured cortical neurons from *Hdh*$^{Q7/Q140}$ HD-knock-in mice. The neurons were treated with the indicated compounds (100 nM for 10O5, 8F20 and AN1; 50 nM for AN2) with or without the autophagy inhibitor NH_4Cl (top) or chloroquine (bottom left), or the autophagy activator rapamycin (bottom right). The same amount of culture medium was added in the controls (top). The statistical analysis was performed by one-way ANOVA with post hoc Dunnett's tests, and the *F*, degree of freedom and post hoc *P* values are indicated in each bar plot. **b**, Western blots using indicated HTT or polyQ antibodies for samples from cultured cortical neurons treated with the indicated compounds: 10O5 (100 nM), 8F20 (100 nM) or AN2 (50 nM). The HTT gel blots presented in Fig. 2d (right) were cropped from first four blots. The low molecular weight bands were run out in these blots so that the wtHTT and mHTT could be better separated. Note that the weak bands just above 250 kDa in the first two blots were leftover signals from the spectrin blotting. The spectrin signals were too strong to be stripped completely. **c**, Western blots using the antibody MW1 or 3B5H10, which detects mHTT specifically. We ensured that the relatively low-molecular-weight proteins did not run out of the gels. No increase of potential polyQ-containing mHTT N-terminal fragments was observed. **d**, iPS-cell-derived striatal neurons from a patient with HD (Q47) were treated with the indicated compounds (100 nM, with 0.1% DMSO) in presence of an additional 0.1% DMSO or 10 mM NH_4Cl, and the mHTT levels were measured by HTRF using the 2B7/MW1 antibody pair. All signals were normalized to the averaged signals from the DMSO control group. The statistical analysis was performed by one-way ANOVA with post hoc Dunnett's tests, and *F*, degree of freedom and post hoc *P* values are indicated in each bar plot. ****$P < 0.0001$. The post hoc analysis was not performed if the ANOVA tests did not show significance ($P > 0.05$). **e**, Immortalized fibroblasts from a patient with HD (Q47) were transfected with the non-targeting control siRNA (Neg siRNA) or the ATG5 siRNA (target sequence, GCCUGUAUGUACUGCUUUA; *ATG5* mRNA was knocked down to 17.7 ± 3.0%, $n = 3$, as tested by reverse transcription with quantitative PCR), and then treated after 24 h with the indicated compounds (100 nM) for a further 48 h. mHTT levels were then measured by HTRF using the 2B7/MW1 antibody pair. All signals were normalized to the averaged signals from the DMSO control group. The statistical analysis was performed by one-way ANOVA with post hoc Dunnett's tests, and *F*, degree of freedom and post hoc *P* values are indicated in each bar plot. ****$P < 0.0001$. The post hoc analysis was not performed if the ANOVA tests did not show significance ($P > 0.05$). The western blot of LC3 confirmed the partial inhibition of autophagy in the ATG5-knockdown cells. **f**, Similar to **e**, but in wild-type (WT) or Atg5-knockout (Atg5 KO) mouse embryonic fibroblast lines (MEF) transfected with full-length mHTT (flHTT-Q73). The western blot of LC3 confirmed the inhibition of autophagy in the Atg5-KO cells. For all panels, *n* indicates the number of independently plated wells, and bars represent mean and s.e.m. Full-blots of cropped gels are shown in Supplementary Fig. 1.

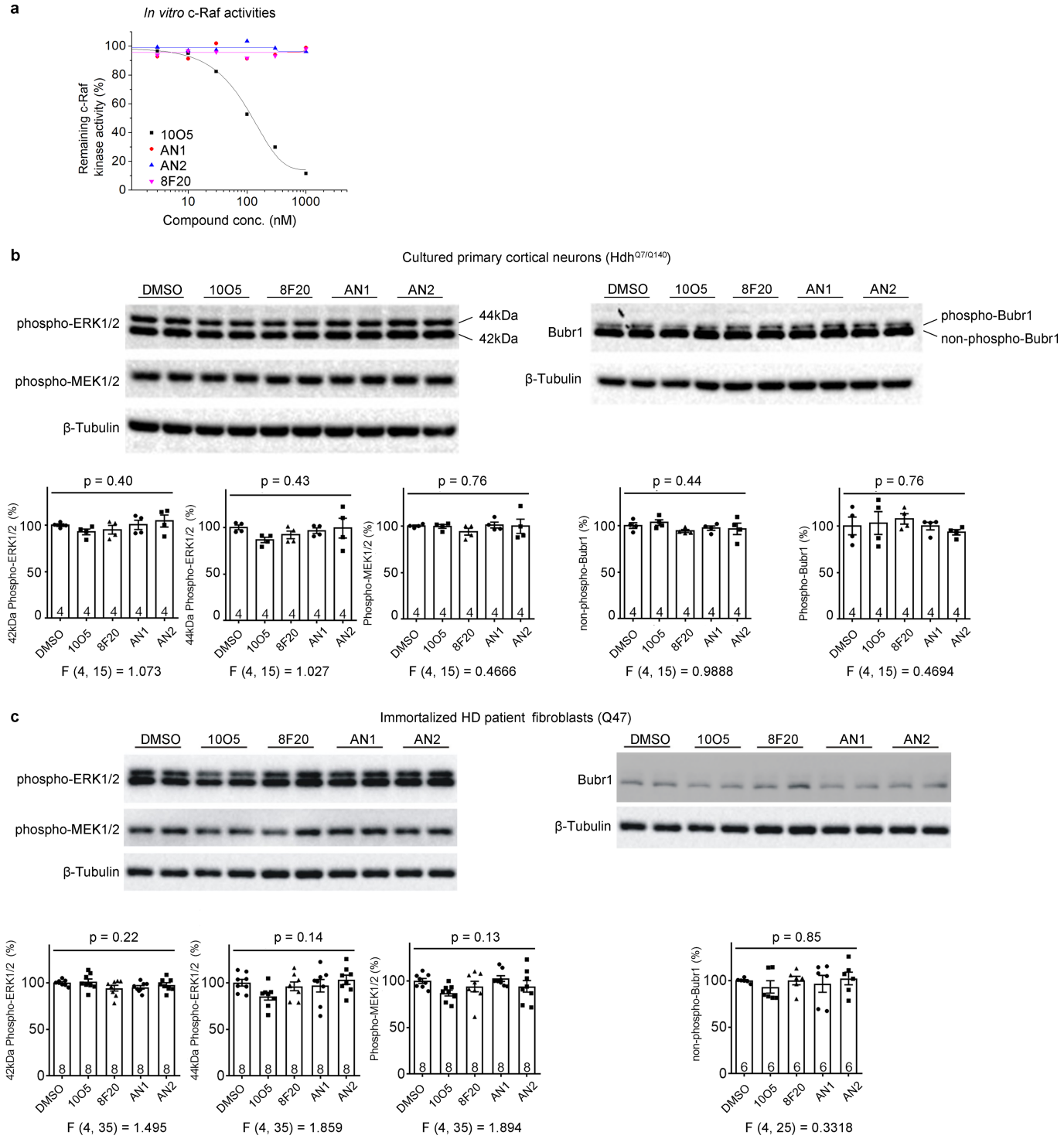

Extended Data Fig. 4 | Potential influence on c-Raf and KSP pathways following treatment with the mHTT–LC3 linker compounds. **a**, Representative results (from three biological repeats) of the in vitro c-Raf kinase assay (see Methods) showing that only 10O5 inhibits c-Raf activity within the concentration range tested. **b**, Representative western blots and quantifications of phospho-MEK and phospho-ERK as indicators of Raf activity (left) and phospho-BUBR1 as an indicator of KSP inhibition (right) in cultured cortical neurons treated with indicated compounds (100 nM for 10O5, 8F20, AN1, and 50 nM for AN2) or the DMSO control. **c**, Similar to **b**, but in immortalized fibroblasts from a patient with HD (Q47). Note that phospho-BUBR1 is essentially absent and too weak to quantify, indicating that KSP was not inhibited by any of the compounds at the concentration tested. Data are mean ± s.e.m. In **b**, **c**, all data were corrected by the loading control (β-tubulin) and normalized to the averaged signal of the DMSO control group. The statistical analysis was performed by one-way ANOVA and *F*, degree of freedom and post hoc *P* values are indicated in each bar plot. The *n* number indicates the number of independently plated and treated wells.

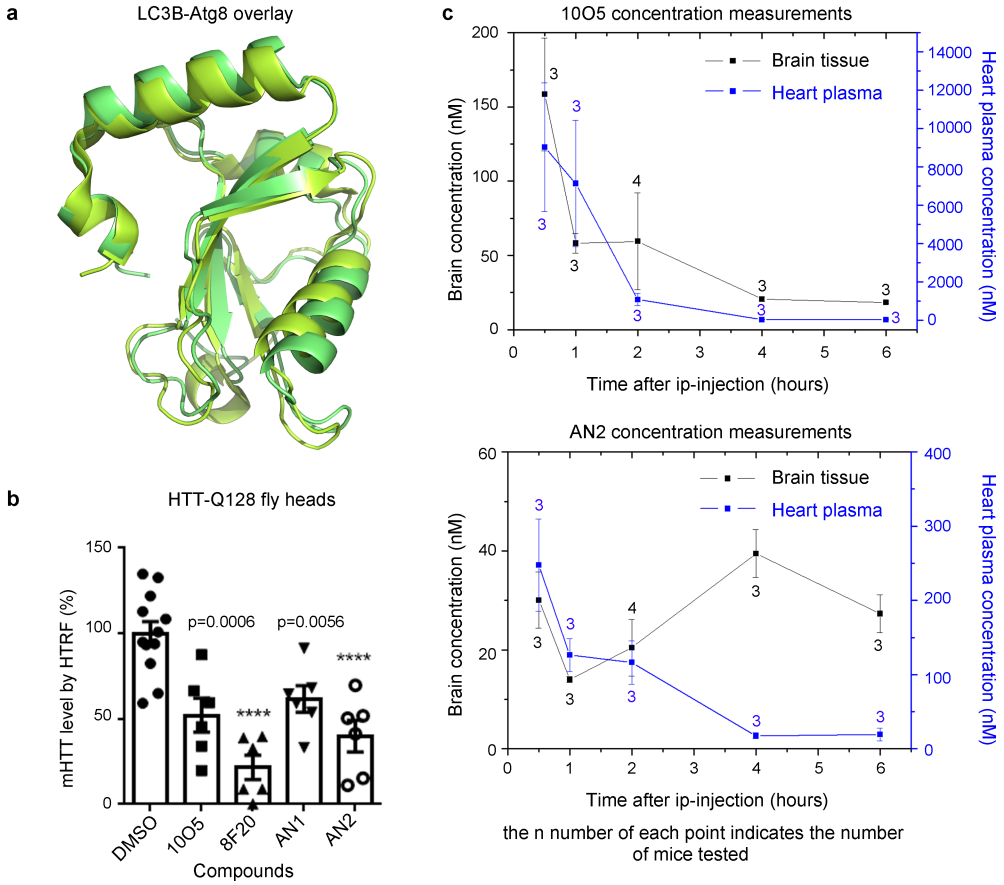

Extended Data Fig. 5 | mHTT-LC3 linker compounds lowered mHTT in transgenic HD flies. a, Overlay between LC3B and predicted Atg8 structure showing high structural similarities. **b**, Transgenic flies expressing full-length HTT(Q128) driven by *elav*-GAL4 were fed with indicated compounds at 10 μM for 6 days, and protein lysates were extracted from the heads. mHTT was then measured by HTRF using the 2B7/MW1 antibody pair. Each dot represents the HTRF signal from each individual sample extracted from five fly heads. All the data were normalized to the average of the DMSO-fed control samples. The statistical analysis was performed by one-way ANOVA and Dunnett's post hoc tests. $F(4, 31) = 15.67$; $^{****}P < 0.0001$. **c**, 10O5 (top) and AN2 (bottom) concentrations in heart plasma and brain tissues were measured by mass spectrometry at the indicated time points for compound-injected mice (0.5 mg kg^{-1}). In the brain tissue, the 10O5 concentrations were ~20 to ~200 nM, and the AN2 concentrations were ~20 to ~40 nM, close to the effective doses that were capable of lowering mHTT in cultured neurons. Data are mean ± s.e.m.

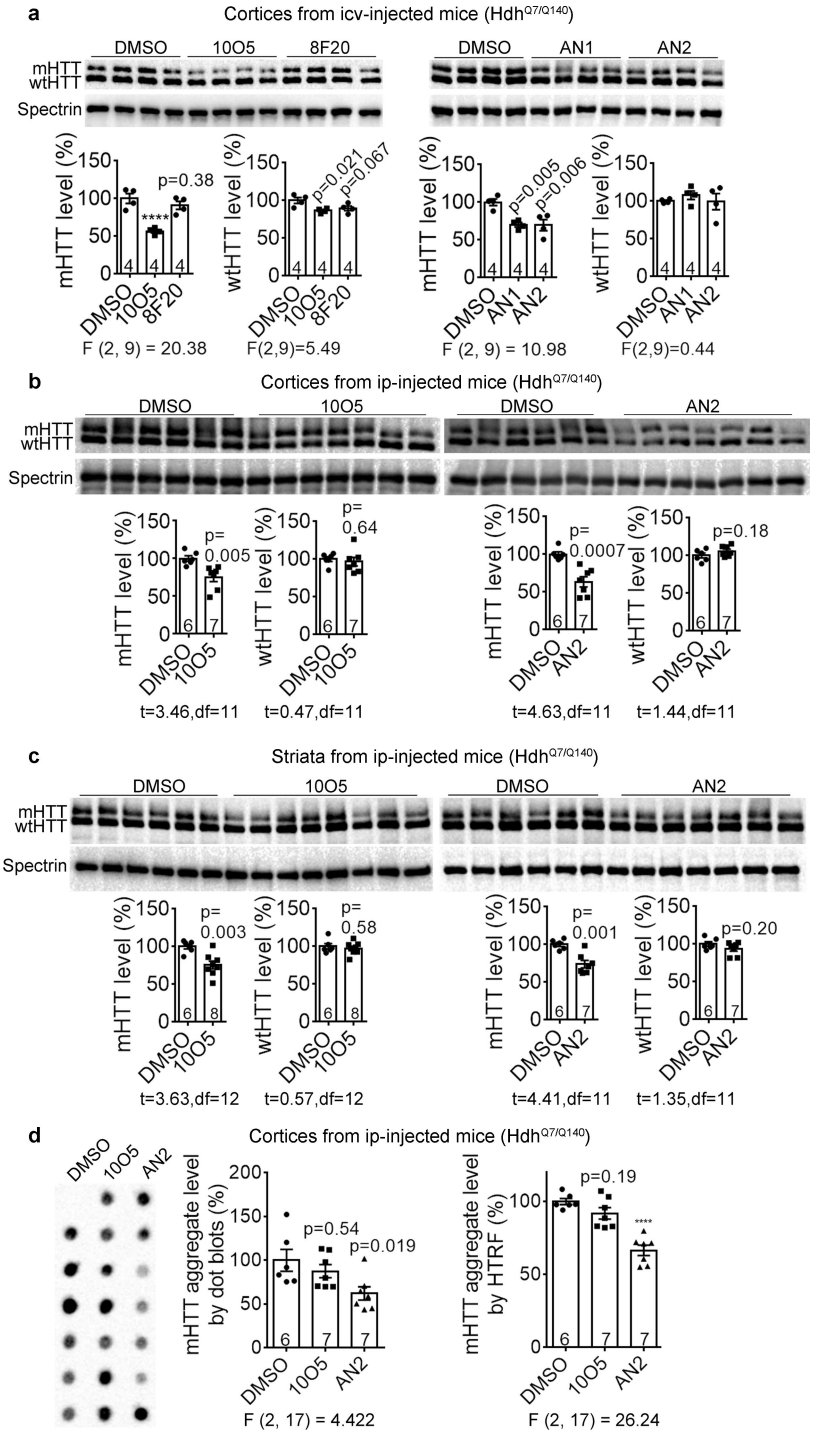

Extended Data Fig. 6 | mHTT–LC3 linker compounds lowered mHTT in vivo in mouse brains. a, Western blots (4 mice (3 months old) for each group) and quantifications of mHTT and wtHTT in the cortices from *Hdh*$^{Q7/Q140}$-knock-in mice with intracerebroventricular injection of the indicated compounds (2 µl at 25 µM for each mouse) for 10 days at one dose per day. HTT was detected by western blot using the 2166 antibody, and the statistical analysis was performed by one-way ANOVA and post hoc Dunnett's tests. *F*, degree of freedom and post hoc *P* values are indicated below each bar plot. **b**, Similar to **a**, except that the compounds were delivered to 5-month-old *Hdh*$^{Q7/Q140}$ mice by intraperitoneal injection (0.5 mg kg^{-1}) for 14 days at one dose per day. **c**, Similar to **b**, but from striata of intraperitoneally injected mice. The mice were injected at 10 months old for 14 days at one dose per day. **d**, Left, representative dot blot results (from two technical replicates) of the protein lysates from **b** using the 4C9 antibody, which preferentially detects mHTT aggregates[23]. Middle, quantification of the dot blots based on the averaged signals from two technical replicates. Right, measurement of mHTT aggregates by the 4C9–4C9 HTRF assay[23]. In all panels, *n* indicates the number of mice tested, and bars represent mean and s.e.m. For quantification, two to three technical replicates were averaged for each mouse. Statistical analysis was performed by one-way ANOVA with post hoc Dunnett's tests, and *F*, degree of freedom and post hoc *P* values are indicated in each bar plot.

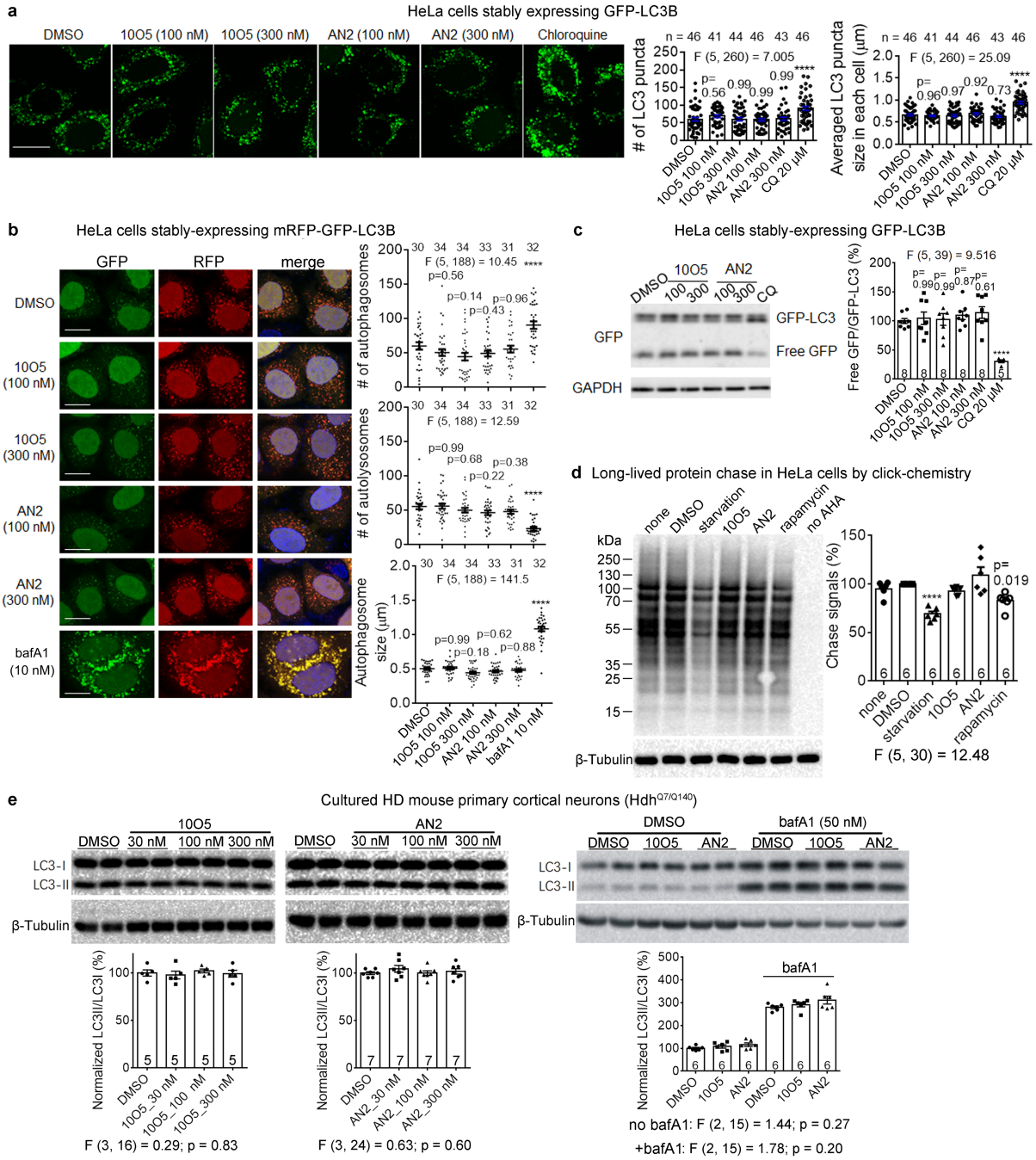

Extended Data Fig. 7 | See next page for caption.

Extended Data Fig. 7 | mHTT–LC3 linker compounds did not influence autophagy. a, HeLa cells stably expressing GFP–LC3B were treated with 2 µl vehicle (0.1% DMSO), 10O5 or AN2 for the indicated concentration for 24 h; chloroquine (CQ, 20 µM) treatment was used as a control. After 24 h, cells were fixed and images were acquired by confocal microscopy. The number and size of GFP vesicles per cell was determined using ImageJ software (*n* indicated on top of each plot). For each treatment, more than 20,000 puncta were quantified (~100 puncta per cell from 226 cells). Scale bar, 10 µm. **b**, Representative images and quantifications of the numbers of autophagosomes (GFP^+ puncta) and autolysosomes (RFP^+GFP^- puncta) in HeLa cells stably expressing mRFP–GFP–LC3B. Scale bar, 10 µm. Autophagosome numbers or sizes were not influenced by 10O5 and AN2 at the indicated concentrations after 24 h treatment (or 4 h treatment, not shown). The autophagsome fusion was also unaffected as indicated by the autolysosome number. Note that the autophagosome and autolysosome numbers and sizes were based on image analysis of the puncta, some of which may represent multiple vesicles. Green vesicles are considered to be autophagosomes (GFP^+ puncta) and red vesicles are considered to be both autophagosomes and autolysosomes. The number of autolysosomes (RFP^+GFP^- puncta) was calculated by subtracting the number of green vesicles from that of the red vesicles. More than 10,000 puncta from 194 cells were analysed. **c**, Representative western blots and quantifications of HeLa cells stably expressing GFP–LC3B. The 'free GFP' was generated by lysosomal cleavage, and thus the free GFP/GFP–LC3B ratio was used as an index for autophagy flux, which was unaffected by 10O5 or AN2, but decreased by the autophagy flux inhibitor chloroquine. **d**, Representative western blots and quantifications of the chase signal of long-lived proteins in HeLa cells as an indicator of autophagy flux (see Methods). Consistent with previous reports[33], starvation reduced the long-lived protein chase signal, whereas rapamycin treatment had a milder effect. The mHTT–LC3 linker compounds 10O5 and AN2 had no influence in this assay. **e**, Representative western blots and quantifications of LC3 in cultured cortical neurons treated with the indicated compounds. Normalized LC3-II/LC3-I was used as the indicator of autophagy. Right blot: 10O5, 100 nM; AN2, 50 nM. **f**, SQSTM1 (p62) levels were determined by western blot for the cortical tissues from mice injected with the indicated compounds or DMSO control. Bars indicate mean and s.e.m.; *n* indicated in each bar shows the number of cells (**a**, **b**), the number of independently plated wells (**c**–**e**) or the number of mice (**f**). Data are mean ± s.e.m. The statistical analysis was performed by one-way ANOVA with post hoc Dunnett's tests (**a**–**e**) or two-tailed unpaired *t*-tests (**f**). Note that the post hoc tests were not performed if the ANOVA tests failed to show significance. $^{****}P < 0.0001$ (post hoc test).

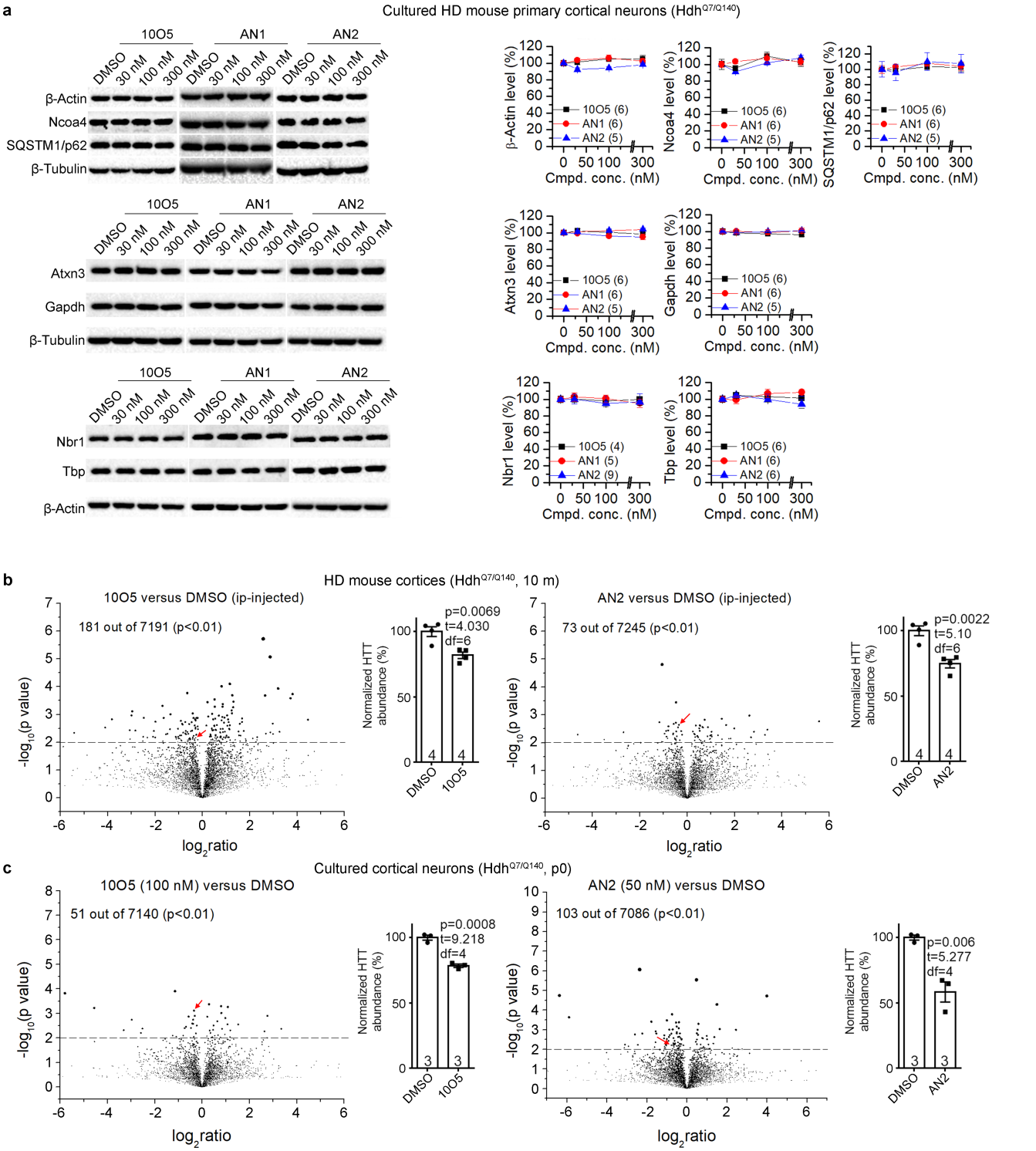

Extended Data Fig. 8 | Investigation on the specificity of mHTT-lowering effects of mHTT–LC3 linker compounds. a, Representative western blots and quantifications of cultured cortical neurons treated with the indicated compounds. None of the proteins tested showed a clear effect (>10%). **b**, Volcano plots of the proteomics analysis of cortices from intraperitoneally injected HD mice (10 month old, 4 mice per group, injected for 14 days). Mice were injected with 0.5 mg kg^{-1} protein with 110 µg kg^{-1} DMSO, and equal amount of vehicle containing DMSO was injected in the control mice. Only proteins detected in both groups of samples used for comparisons were calculated and plotted. Red arrows indicate HTT. See Supplementary Table 2 for complete datasets. The bar plots indicate the total HTT levels normalized to the DMSO control. The actual mHTT reduction is anticipated to be higher, because the compounds reduced mHTT in an allele-selective manner. **c**, Similar to **b**, but in cultured cortical neurons (from postnatal day 0 pups, three wells per group). See Supplementary Table 3 for complete datasets. In all panels, data are mean ± s.e.m.

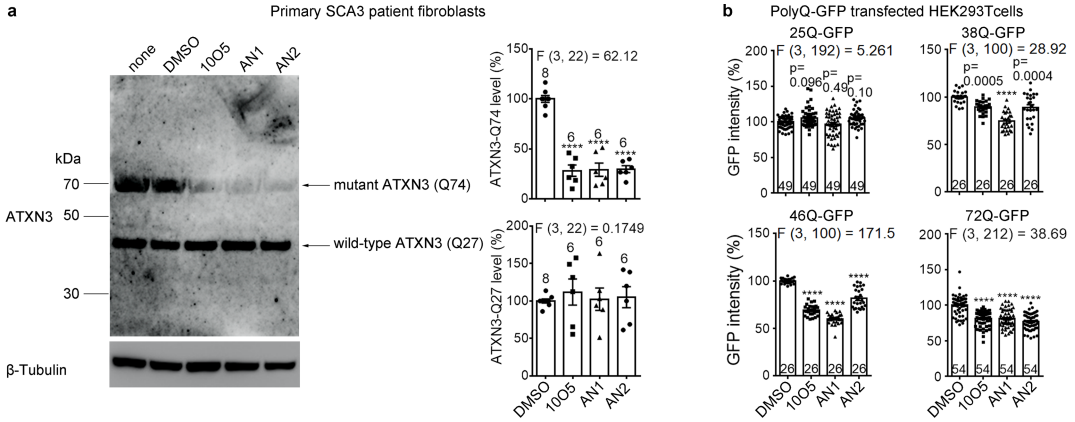

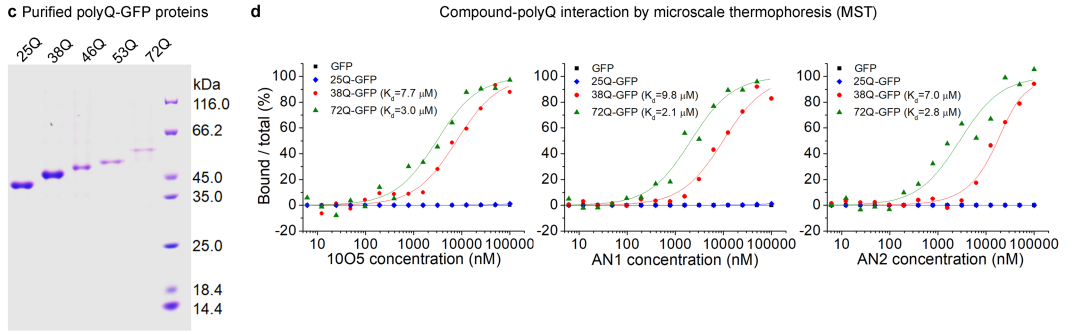

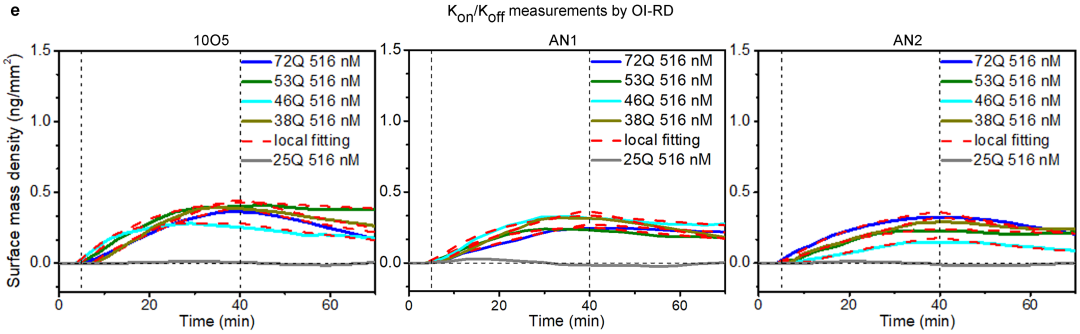

	K_{on} $(min{\cdot}nM)^{-1}$	K_{off} $(min)^{-1}$	K_d (nM)
72Q	8.37×10^{-5}	1.51×10^{-2}	180.4
53Q	1.51×10^{-4}	3.78×10^{-3}	25.0
46Q	3.04×10^{-4}	1.83×10^{-2}	60.2
38Q	1.06×10^{-5}	2.03×10^{-2}	1915.1

	K_{on} $(min{\cdot}nM)^{-1}$	K_{off} $(min)^{-1}$	K_d (nM)
72Q	2.23×10^{-5}	7.94×10^{-3}	356.1
53Q	1.25×10^{-4}	1.35×10^{-2}	108.0
46Q	1.29×10^{-4}	7.67×10^{-3}	59.5
38Q	8.72×10^{-6}	2.62×10^{-2}	3004.6

	K_{on} $(min{\cdot}nM)^{-1}$	K_{off} $(min)^{-1}$	K_d (nM)
72Q	6.20×10^{-5}	1.92×10^{-2}	309.7
53Q	1.08×10^{-4}	4.65×10^{-3}	43.1
46Q	7.65×10^{-6}	2.57×10^{-2}	3359.5
38Q	2.99×10^{-6}	1.5×10^{-2}	5016.7

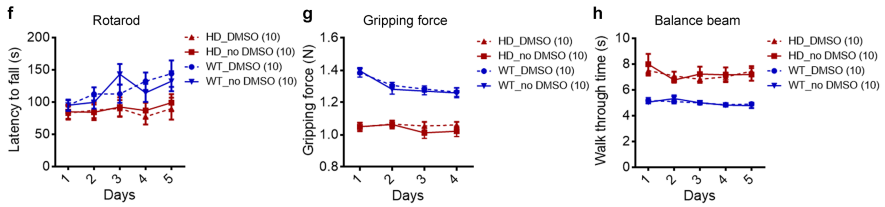

Comparisons (F (3, 180) = 9.015)	p values	
WT no DMSO vs. WT DMSO	ns	0.992
HD_no DMSO vs. HD_DMSO	ns	0.964
WT no DMSO vs. HD no DMSO	**	0.007
WT DMSO vs. HD DMSO	***	0.0005

Comparisons (F (3, 144) = 134.4)	p values	
WT no DMSO vs. WT DMSO	ns	0.973
HD_no DMSO vs. HD_DMSO	ns	0.681
WT no DMSO vs. HD no DMSO	****	<0.0001
WT DMSO vs. HD DMSO	****	<0.0001

Comparisons (F (3, 180) = 69.32)	p values	
WT no DMSO vs. WT DMSO	ns	0.999
HD_no DMSO vs. HD_DMSO	ns	0.971
WT no DMSO vs. HD no DMSO	****	<0.0001
WT DMSO vs. HD DMSO	****	<0.0001

Extended Data Fig. 9 | See next page for caption.

Extended Data Fig. 9 | mHTT–LC3 linker compounds lowered the mutant ATXN3 protein with polyQ expansion in an allele-selective manner. **a**, Representative western blots and quantifications of ATXN3 levels in a fibroblast line from a patient with SCA3 treated with the indicated compounds. The lowering of mutant (Q74) but not wild-type (Q27) ATXN3 was observed by treatment of linker compounds tested. **b**, Quantification of the GFP intensity as an indicator of polyQ–sfGFP (25Q–GFP, 38Q–GFP, 46Q–GFP and 72Q–GFP) protein levels in transfected HEK293T cells treated with the indicated compounds using Incucyte. Reduction of 72Q–GFP, 46Q–GFP and 38Q–GFP but not 25Q-GFP was observed. In **a** and **b**, the compound concentrations were 100 nM for 10O5 and AN1, and 50 nM for AN2. Bar plots present mean ± s.e.m., and *n* indicates the number of independently plated wells. **c**, SDS–PAGE analysis of polyQ–sfGFP proteins (25Q, 38Q, 46Q, 53Q and 72Q) purified from HEK293T cells. The protein purification methods were similar to those for HTT proteins. **d**, Binding of 10O5, AN1 and AN2 to sfGFP (GFP) or different polyQ–sfGFP (25Q–GFP, 38Q–GFP and 72Q-GFP) proteins in standard treated capillaries measured by MST, performed and analysed similarly as in Extended Data Fig. 2b. All these compounds interact with 38Q–GFP and 72Q–GFP but not with 25Q–GFP or GFP. **e**, Association–dissociation curves of surface-immobilized compounds 10O5, AN1 and AN2 with polyQ–sfGFP (72Q, 53Q, 46Q, 38Q and 25Q) proteins. For all association–dissociation curves, vertical dashed lines mark the starts of association and dissociation phases of the binding event. The red dashed curves are fits to a Langmuir reaction model with the fitting parameters listed at the bottom of each plot. No binding signals were observed for 25Q–sfGFP (25Q). **f**–**h**, Results of mouse behavioural test performed similarly to those in Fig. 5d–f, except that the mice were injected with saline (0.9% NaCl) with DMSO (110 μg kg^{-1}) or without DMSO. The statistical analysis was performed by two-way ANOVA with post hoc Bonferroni's tests, and *F*, *P* values and degrees of freedom are indicated in the table below each plot. In all panels, data are mean ± s.e.m.

Extended Data Table 1 | Summary of data on mHTT lowering or rescue of HD-relevant phenotypes

Model and treatment	Readout and figures	Compound effects
cultured primary cortical neurons, from mice ($Hdh^{Q7/Q140}$)	the mHTT level by Western-blot (Fig. 2a&d)	10O5: 26.0±3.3% lowering
		8F20: 40.1±12.6% lowering
		AN1: 35.7±2.8% lowering
		AN2: 34.0±6.2% lowering
primary human HD patient fibroblasts (Q49)	the mHTT level by HTRF (Fig. 3a)	10O5: 45.1±4.0% lowering
		8F20: 44.8±4.9 lowering
		AN1: 46.1±6.2% lowering
		AN2: 54.8±7.5% lowering
primary human HD patient fibroblasts (Q55)	the mHTT level by HTRF (Fig. 3a)	10O5: 34.3±5.4% lowering
		8F20: 28.7±3.6% lowering
		AN1: 26.5±7.0% lowering
		AN2: 39.3±4.8% lowering
primary human HD patient fibroblasts (Q68)	the mHTT level by HTRF (Fig. 3a)	10O5: 20.9±2.7% lowering
		8F20: 22.9±5.3% lowering
		AN1: 26.4±2.8% lowering
		AN2: 18.1±5.1% lowering
HD patient iPSC-derived neurons (Q47)	the mHTT level by HTRF (Ext. Data. Fig. 5c)	10O5: 31.4±3.2% lowering
		8F20: 28.9±3.7% lowering
		AN1: 39.3±3.2% lowering
		AN2: 40.5±2.8% lowering
	surface area of each neuron by Tuj1 staining (Fig. 5a)	10O5: 69.5±1.6% rescue
		8F20: 51.6±3.1% rescue
		AN1: 58.8±4.9% rescue
		AN2: 64.4±2.7% rescue
immortalized human HD patient fibroblasts (Q47)	the mHTT level by HTRF (Fig. 3b)	10O5: 30.2±4.5% lowering
		8F20: 22±4.8% lowering
		AN1: 42.0±3.9% lowering
		AN2: 41.4±5.1% lowering
icv-injected mice ($Hdh^{Q7/Q140}$)	the mHTT level by Western-blot (Ext. Data Fig. 9a)	10O5: 43.3±2.2% lowering
		8F20: 9.1±5.3% lowering (n.s.)
		AN1: 29.9±2.9% lowering
		AN2: 30.3±7.4% lowering
ip-injected mice ($Hdh^{Q7/Q140}$)	the cortical mHTT by Western-blot (Ext. Data Fig. 9b)	10O5: 24.8±4.2% lowering
		AN2: 36.6±7.4% lowering
	the striatal mHTT by Western-blot (Ext. Data Fig. 9c)	10O5: 22.9±2.3% lowering
		AN2: 26.3±5.5% lowering
	the cortical HTT by MASS-SPEC (Ext. Data Fig. 11b)	10O5: 18.1±2.4% lowering
		AN2: 25.2±3.2% lowering
	latency to fall by rotarod tests (Fig. 5d)	10O5: (60.8% averaged rescue)
		AN2: (64.3% averaged rescue)
	passing time by balance beam tests (Fig. 5e)	10O5: (77.2% averaged rescue)
		AN2: (92.8% averaged rescue)
	gripping force tests (Fig. 5f)	10O5: (43.6% averaged rescue)
		AN2: (52.4% averaged rescue)

A summary table showing the percentage lowering of mHTT or HTT levels, and the percentage rescue of HD-relevant phenotypes (normalized to the difference between HD and wild type) in different HD models assayed by different approaches under optimal conditions. The corresponding data are indicated in the middle column. The percentage change/rescue is presented as mean ± s.e.m.

nature research

Corresponding author(s): Boxun Lu, Yiyan Fei, Yu Ding

Reporting Summary

Nature Research wishes to improve the reproducibility of the work that we publish. This form provides structure for consistency and transparency in reporting. For further information on Nature Research policies, see Authors & Referees and the Editorial Policy Checklist.

Statistical parameters

When statistical analyses are reported, confirm that the following items are present in the relevant location (e.g. figure legend, table legend, main text, or Methods section).

n/a	Confirmed	
☐	☒	The exact sample size (*n*) for each experimental group/condition, given as a discrete number and unit of measurement
☐	☒	An indication of whether measurements were taken from distinct samples or whether the same sample was measured repeatedly
☐	☒	The statistical test(s) used AND whether they are one- or two-sided *Only common tests should be described solely by name; describe more complex techniques in the Methods section.*
☐	☒	A description of all covariates tested
☐	☒	A description of any assumptions or corrections, such as tests of normality and adjustment for multiple comparisons
☐	☒	A full description of the statistics including central tendency (e.g. means) or other basic estimates (e.g. regression coefficient) AND variation (e.g. standard deviation) or associated estimates of uncertainty (e.g. confidence intervals)
☐	☒	For null hypothesis testing, the test statistic (e.g. *F*, *t*, *r*) with confidence intervals, effect sizes, degrees of freedom and *P* value noted *Give P values as exact values whenever suitable.*
☒	☐	For Bayesian analysis, information on the choice of priors and Markov chain Monte Carlo settings
☒	☐	For hierarchical and complex designs, identification of the appropriate level for tests and full reporting of outcomes
☐	☒	Estimates of effect sizes (e.g. Cohen's *d*, Pearson's *r*), indicating how they were calculated
☐	☒	Clearly defined error bars *State explicitly what error bars represent (e.g. SD, SE, CI)*

Our web collection on statistics for biologists may be useful.

Software and code

Policy information about availability of computer code

Data collection	All data collection softwares came with the equipment utilized for experiments, including IncuCyte 2011A, MO. Control (NT.115), PerkinElmer EnVision Manager Version 1.13, HKL2000 V719, Image Lab Version 3.0, ZEN 2.3
Data analysis	The softwares utilized for analysis were all commercially available or could be downloaded from open source, including GraphPad Prism 7, ImageJ 1.52a, Origin8, Microsoft Excel 2016, PASS 16, Nanotemper analysis (1.5.41) , PyMOL 2.2, HKL2000, Phaser 2.8, Mascot 2.3, PASS 16, IncuCyte 2011A, MO.Affinity Analysis (NT.115).

For manuscripts utilizing custom algorithms or software that are central to the research but not yet described in published literature, software must be made available to editors/reviewers upon request. We strongly encourage code deposition in a community repository (e.g. GitHub). See the Nature Research guidelines for submitting code & software for further information.

Data

Policy information about availability of data

All manuscripts must include a data availability statement. This statement should provide the following information, where applicable:

- Accession codes, unique identifiers, or web links for publicly available datasets
- A list of figures that have associated raw data
- A description of any restrictions on data availability

The protein structure data has been uploaded to the PDB database with entry number 6J04. The source data in excel files have been provided for all essential plots in the figures. The full gel blots and the proteomics datasets have been provided as supplementary tables. All the other data are available from the authors upon request.

Field-specific reporting

Please select the best fit for your research. If you are not sure, read the appropriate sections before making your selection.

☒ Life sciences ☐ Behavioural & social sciences ☐ Ecological, evolutionary & environmental sciences

For a reference copy of the document with all sections, see nature.com/authors/policies/ReportingSummary-flat.pdf

Life sciences study design

All studies must disclose on these points even when the disclosure is negative.

Sample size	To ensure to reach a statistical power>0.8, power analyses were performed for each assay based on estimated values by PASS 16 (https://www.ncss.com/software/pass/) before experiments. Estimation was based on our previously published results on similar experiments and preliminary experiments. The power analysis suggested n > =3 for mHTT level measurements and n > =5 for behavioral experiments. In all the experiments we performed, we have used a larger n than these numbers, and we also performed post-experiment power analyses to ensure that power > 0.8 for all the significant differences.
Data exclusions	Data were not excluded unless clear experimental failures occurred, including cell contamination, gel transfer failures and lack of signals in positive controls. The exclusion criteria were pre-established.
Replication	All experimental data was reliably reproduced in multiple independent experiments as indicated in the figure legends. The protein-compound interaction experiments and the HTT-lowering experiments have been replicated by at least two independent researchers.
Randomization	For the in vivo experiments in the mouse, randomization was performed by assigning random numbers. For the Drosophila experiments, the flies were randomly distributed into the vials after anesthesia.
Blinding	As indicated in the figure legends, the investigators were blinded during data collection and analysis where possible, included immunofluorescence experiments, drug treatment experiments in mouse and fly models for HTT level measurements and behavioral assays.

Reporting for specific materials, systems and methods

Materials & experimental systems

n/a	Involved in the study
☐	☒ Unique biological materials
☐	☒ Antibodies
☐	☒ Eukaryotic cell lines
☒	☐ Palaeontology
☐	☒ Animals and other organisms
☐	☒ Human research participants

Methods

n/a	Involved in the study
☒	☐ ChIP-seq
☒	☐ Flow cytometry
☒	☐ MRI-based neuroimaging

Unique biological materials

Policy information about availability of materials

Obtaining unique materials	All unique materials (some of the patient fibroblast lines) are readily available from the authors.

Antibodies

Antibodies used

Anti-β-tubulin (Abcam, cat. no. ab6046, lot no. GR3209100-1, 1:10000)
Anti-TUBB3 (Biolegends (Covance), cat. no. 801202, clone TUJ1, lot no. B2335555, 1:500)
Anti-ATXN3 (Millipore, cat. no. MAB5360, clone no. 1H9, lot no. 3096481,1:1000):
Anti-Gapdh (Proteintech, cat. no. 60004-1, lot no. 10004129, 1:5000)
Anti-NBR1 (ThermoFisher Scientific, cat. no. PA5-54660, lot no. SJ2462971A, 0.4 μg/mL)
Anti-β-actin (Beyotime, cat.no. AA128, clone no.AC-74, lot no. 031918180821, 1:1000)
Anti-TBP antibody (Abcam, cat. no. ab818, clone no.1TBP18, lot no. GR315577-3, 1:1000)
Anti-SQSTM1 antibody (ThermoFisher Scientific, cat.no. PA5-27247, lot no. SC2360851N, 1:1000)
Anti-spectrin antibody (Millipore, cat.no. MAB1622, clone no. AA6, lot no. 2943221, 1:2000)
Anti-Ncoa4 antibody (Santa cruz, cat.no. sc-373739, clone no. C-4, 1:200)
Anti-GST antibody (ProteinTech, cat.no. HRP-66001, clone no. 3G12B10, lot no. 20000091, 1:2000)
anti-MBP antibody (ProteinTech, cat.no. 15089-1-AP, lot no. 00058716, 1:3000)
Anti-His antibody (Beyotime, cat. no. AH367, clone no.AD1.1.10, lot no.011018180312, 1:100)
Anti-LC3B antibody (ThermoFisher Scientific, cat.no.PA1-16930, lot no.T12629311, 1:1000; ThermoFisher Scientific, cat.no. 700712, clone no. 2H30L32, lot no. 2086347, 1:200)
Phospho-Erk1/2 Pathway Sampler Kit (Cell Signaling Technology cat.no.9911, 1:1000; Phospho-MEK1/2, clone no.41G9, lot no.18, Phospho-p44/42 MAPK, clone no.D13.14.4E, lot no.24)
Anti-GFP (Cell Signaling Technologies, cat. no. 2956, clone no. D5.1, lot no. 4, 1:1000)
Anti-BubR1 antibody (BD Transduction, cat. no. 612503, clone no. 9/BUBR1, 1:1000)
Anti-Huntingtin Protein antibody 2166 (Millipore, cat. no. MAB2166, clone no.1HU-4C8, lot no. 2943221, 1:1000)
Anti-polyQ antibody 3B5H10 (Sigma, cat. no. P1874, clone no. 3B5H10, lot no. 047M4820V, 1:1000)
Anti-HTT antibody (D7F7)XP (Cell Signaling Technologies, cat. no. 5656s, clone no. D7F7, lot no. 4, 1:1000)
The other HTT antibodies including 2B7, ab1 and MW1 were previously published and characterized by other groups, and they originally obtained from those groups. They were diluted at 1:1000 for Western-blots.

Validation

The anti-β-tubulin antibody has been validated for Western-blots of both human and mouse samples by many previous publications (e.g. PMID: 28869595). The anti-TUBB3 antibody has been validated for immunocytochemistry of human sample by many previous publications (e.g. PMID: 30545851). The anti-ATXN3 antibody has been validated for Western-blots of both human and mouse samples by many several publications (e.g. PMID: 28180282). The anti-Gapdh antibody has been validated for Western-blots of mouse sample by many previous publications (e.g. PMID: 31091447). The anti-NBR1 antibody has been validated for Western-blots of mouse in antibodypedia （https://www.antibodypedia.com/gene/8116/NBR1/antibody/3592759/PA5-54660). Anti-β-actin antibody has been validated for Western-blots of both human and mouse samples by many previous publications (e.g. PMID: 30459625). The anti-TBP antibody has been validated for Western-blots of both human and mouse samples by many previous publications (e.g. PMID: 28280206). The anti-SQSTM1 antibody has been validated for Western-blots of mouse sample by many previous publications (e.g. PMID: 28869595). The anti-spectrin antibody has been validated for Western-blots of both human and mouse samples by many previous publications (e.g. PMID: 28869595). The anti-Ncoa4 antibody has been validated for Western-blots of both human and mouse samples by many previous publications (e.g. PMID: 30630985). The anti-GST antibody and the anti-MBP antibody has been validated for in vitro pull-down and Western-blot by experimental data in this study (Fig 4a-b). Anti-His antibody has been validated for immunostaining by experimental data in this study (Fig 4c). The anti-LC3B antibody (ThermoFisher Scientific, cat.no. PA1-16930) has been validated for Western-blots of mouse sample by vender (https://www.thermofisher.com/cn/zh/antibody/product/LC3B-Antibody-Polyclonal/PA1-16930). The anti-LC3B antibody (ThermoFisher Scientific, ThermoFisher Scientific, cat.no. 700712) has been validated by previous publications for immunostaining in human and mouse cells (PMID: 29151587, 22622129). The anti-GFP antibody has been validated by previous literature (PMID: 31112137; PMID: 31067454; PMID: 30996031). The Phospho-Erk1/2 Pathway Sampler Kit have been validated for Western-blots of mouse sample by several previous publications (e.g. PMID: 29636449). The anti-BubR1 antibody has been validated for Western-blots of both human and mouse samples by many previous publications (e.g. PMID: 27528194). The anti-HTT antibody (D7F7)XP have been validated for Western-blots of both human and mouse samples by many previous publications.(e.g. PMID: 26863614, PMID: 23575829). The other HTT antibodies including 2166, 3B5H10, 2B7, ab1 and MW1 have been validated for Western-blots of both human and mouse samples by many previous publications (e.g. PMID: 25738228). The antibody 2166 has also been validated for immunostaining experiments in mouse samples by this study (Fig. 4d).

Eukaryotic cell lines

Policy information about cell lines

Cell line source(s)

Some of the primary patient fibroblasts were obtained from HD patients (Q47, Q49, Q55) and healthy sibling (WT, Q19) controls in a Mongolian Huntington's disease family. The HD Q68 fibroblast line was obtained from Coriell Cell Repositories (Camden, NJ, USA). The PD line was obtained from an idiopathic Parkinson's disease patient, and the SCA3 line was obtained from a SCA3 patient with the ATXN3 expansion mutation (Q74). The studies were approved by The Ethic Community of Institutes of Biomedical Sciences at Fudan University (#28) for obtaining the HD and wild-type patient fibroblasts, and by Huashan Hospital Institutional Review Board at Fudan University (#174) for obtaining the PD and SCA3 patient fibroblasts. Verbal and written consent was obtained from patients. The procedures were in compliance with all relevant ethical regulations. The immortalized fibroblasts were generated by infection of lentivirus expressing SV40T. For generation of iPS cells (iPSCs), the primary fibroblasts were transduced with the retroviral STEMCCA polycistronic reprogramming system (Millipore, cat. no. SCR548). The iPSCs were confirmed positive for Tra-1-81, Tra-1-60, SSEA-4 and Nanog by immunofluorescence and flow-cytometry. All four vector-encoded transgenes were found to be silenced and the karyotype was normal. iPSC were cultured in E8 medium (ThermoFisher Scientific, cat. no. A1517001) on Matrigel (Corning, cat. no. 354277) surface. iPSCs were differentiated to Pax6-expressing primitive neuroepithelia (NE) for 10-12 days in a neural induction medium. Sonic hedgehog (SHH, 200 ng/ml) was added at days 10-25 to induce ventral progenitors. For neuronal differentiation, neural progenitor clusters were dissociated and placed onto poly-ornithine/laminin-coated coverslips at day

	26 in Neurobasal medium (ThermoFisher Scientific, cat. no. 21103049), with 1× B-27 (ThermoFisher Scientific, cat. no. 17504044), 1× N-2 (ThermoFisher Scientific, cat. no. 17504048), brain derived neurotrophic factor (BDNF, 20 ng/ml, Protech, cat. no. 450-02), glial-derived neurotrophic factor (GDNF, 10 ng/ml, Protech, cat. no. 450-10), insulin-like growth factor 1 (IGF1, 10 ng/ml, Protech, cat. no. 100-11) and Vitamin C (Sigma cat. no. D-0260, 200 ng/ml). The mouse striatal cells (STHdh) were obtained from Coriell Cell Repositories (Camden, NJ, USA). The HEK293T cells and the HeLa cells were originally obtained from American Type Culture Collection (ATCC). Atg5 WT and KO MEFs were from N. Mizushima.
Authentication	The HEK293T and HeLa cell lines were authenticated by Short Tandem Repeat (STR) profiling methods. The Atg5 WT and KO MEFs were obtained directly from the laboratory which generated these cell lines (N. Mizushima), and they were further authenticated by Short Tandem Repeat (STR) profiling methods comparing with primary cultured MEFs. The patient fibroblasts were obtained and cultured from patients, and they were not authenticated.
Mycoplasma contamination	The cells were tested every two months by a TransDetect PCR Mycroplasma Detection Kit (Transgen Biotech, cat. no. FM311-01) to ensure that they are mycoplasma free.
Commonly misidentified lines (See ICLAC register)	HeLa cells were used in the HTT-LC3 colocalization experiments, because it is commonly used cell line for autophagy experiments and it showed more distinct LC3 puncta than other cells that we have tested. In addition, it has high transfection efficiency.

Animals and other organisms

Policy information about studies involving animals; ARRIVE guidelines recommended for reporting animal research

Laboratory animals	The fruitfly experiments used Drosophila Melanogaster, and adult virgin female flies were used for experiments at indicated days of age (ranging from 0 to 50 days old after eclosion). The mouse experiments used the C57BL/6 strain including both male and female of the desired genotype. For icv experiments, the age was 3 months +/- 0 days old; for ip-injection followed by testing of cortical HTT, the age was 5 months +/- 0 days old; for ip-injection followed by testing of striatal HTT, the age was 10 months +/- 3 days old; for ip-injection followed by behavioral analysis, the age was 10 months +/- 3 days old.
Wild animals	The study did not involve wild animals.
Field-collected samples	The study did not involve samples collected from the field.

Human research participants

Policy information about studies involving human research participants

Population characteristics	Since we are testing the compounds in patient cells rather than patient groups, we do not have population characteristics of human participants. For each patient, we cultured many cells from them and treat different group of cells with different compounds to test their effects within each patient cell lines. In general, the patients were diagnosed base on symptoms and genetic testings, and they received no treatment at the time they provided dermal fibroblasts. The HD patients (Q47/Q19, 46-year-old female; Q49/Q19, 44-year-old male; Q55/Q19, 39-year-old male) and the healthy sibling control (Q19/Q19, 39-year-old female) were from a Mongolian family. The The SCA3 patient was a 32 years old female patient when providing the dermal fibroblasts. She first came to the clinic complaining with clumsy and slowness in the lower limbs and left upper limb for 1 year. Her father and grandfather had the same symptoms but had passed away. After a one year follow up, she developed unstable walking. She was diagnosed as spinocerebellar ataxia and confirmed by genetic testing with the repeat number of Q74/Q27 in ATXN3. The PD patient was a 74 years old male patient when providing the dermal fibroblasts. He developed tremor, rigidity and bradykinesia for 6 years. The symptoms started at age 68 and he was diagnosed as PD at age 69 and followed up in our center for 5 years. A panel containing 254 PD and related genes and PD MLPA were carried out in the patient but did not find any known mutations related to PD. DAT-PET CT found the decreased DAT binding in the right caudate nucleus and putamen.
Recruitment	The HD and SCA3 patients were recruited by clinical symptoms and confirmed with genetic testing. The PD patients were recruited by clinical symptoms and confirmed by follow-up visits of more than 5 years and DAT PECT-CT. The recruitment could be biased because only a few patients who see the collaborating doctor and want to donate dermal fibroblasts for potential future research were selected. This is typical for preclinical studies, and our study is comparing different compound treated groups within each of the cell line, and thus not influenced by patient-to-patient variations. Nonetheless, while we have tested multiple patient cells and obtained consistent results, it is still possible that some of the other patient cells show different results.